

Lawrence Berkeley National Laboratory

Recent Work

Title

STUDY OF ROCK SHATTERING BY INTENSE BURSTS OF ENERGETIC ELECTRONS

Permalink

<https://escholarship.org/uc/item/6hm8t8sj>

Author

Avery, Robert T.

Publication Date

1974-05-01

RECEIVED
LAWRENCE
RADIATION LABORATORY

LBL-3019
c. 2

JUN 26 1974

LIBRARY AND
DOCUMENTS SECTION

STUDY OF ROCK SHATTERING BY
INTENSE BURSTS OF ENERGETIC ELECTRONS

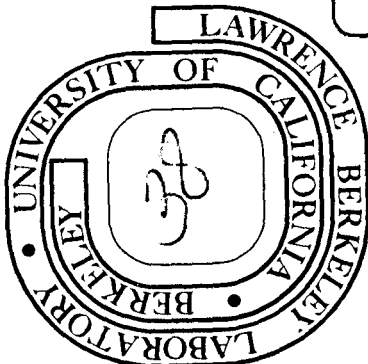
Robert T. Avery
(D. Eng. Thesis)

May 1974

Prepared for the U. S. Atomic Energy Commission
under Contract W-7405-ENG-48 and with the financial
support of the National Science Foundation
under NSF Grant AG-393

TWO-WEEK LOAN COPY

*This is a Library Circulating Copy
which may be borrowed for two weeks.
For a personal retention copy, call
Tech. Info. Division, Ext. 5545*



LBL-3019
c. 2

DISCLAIMER

This document was prepared as an account of work sponsored by the United States Government. While this document is believed to contain correct information, neither the United States Government nor any agency thereof, nor the Regents of the University of California, nor any of their employees, makes any warranty, express or implied, or assumes any legal responsibility for the accuracy, completeness, or usefulness of any information, apparatus, product, or process disclosed, or represents that its use would not infringe privately owned rights. Reference herein to any specific commercial product, process, or service by its trade name, trademark, manufacturer, or otherwise, does not necessarily constitute or imply its endorsement, recommendation, or favoring by the United States Government or any agency thereof, or the Regents of the University of California. The views and opinions of authors expressed herein do not necessarily state or reflect those of the United States Government or any agency thereof or the Regents of the University of California.

CONTENTS

	<u>Page</u>
Abstract	iii
1. Introduction	1
2. "Thermal Crater" Fracturing	3
2.1 Description and analysis	3
2.2 Thermal Crater Experiments	13
2.3 Discussion of Thermal Crater Fracturing	13
3. "Shock Spalling" Technique	18
3.1 Description	18
3.2 Shock Spalling Experiments	18
3.2.1 Febetron tests	20
3.2.2 Tests at Astron	20
3.2.3 Tests using Pulserad 422 accelerator	23
3.2.4 Tests using Pulserad 1140 accelerator	41
3.2.5 Tests using Hermes II accelerator	47
3.2.6 Summary of experimental observations	67
3.3 Analysis and discussion of the shock spalling technique	68
4. Prospects for the Future	76
5. Conclusions	81
Acknowledgments	83
References	84
Appendix A - Electron Bombardment Heating of Interstitial Water	A-1

STUDY OF ROCK SHATTERING BY
INTENSE BURSTS OF ENERGETIC ELECTRONS

Doctor of
Engineering

Robert Tolman Avery
Lawrence Berkeley Laboratory
University of California

Mechanical
Engineering


Chairman of Committee

ABSTRACT

Tests have demonstrated that an intense short-duration pulse of energetic (≥ 1 MV) electrons can produce significant volume removal in a variety of rocks. Test results, together with discussion of the associated microsecond fracture processes, are presented. The prospects of applying this technique to rapid tunneling through hard rock are briefly discussed.

Rock samples ranging from very hard to soft were tested, including greenstone, granite, basalt, limestone, sandstone, shale and damp adobe clay. Removal of rock from the face was demonstrated on all types. In general, for the same energy input, softer rock shows greater spall volume than hard rock and wet rock exhibits greater spall volume than dry rock. The spall debris is of fine nature, being either sand, dust or small flakes. Spall volumes of typically one to almost a hundred cubic centimeters are produced by a single burst of electrons of less than one microsecond duration and having from 3 to 64 kilojoules of energy content. This technique has been labeled "shock spalling."

The electrons deposit substantially all of their energy content as an impulse of heat within the volume of rock immediately below the rock surface. The restrained thermal expansion produces a compressive stresswave which reflects from the free front surface as a tensile stresswave of short time duration ($\sim 1 \mu\text{s}$). Spalling due to this tensile stresswave appears to be the dominant fracture mechanism. Calculations indicate that the magnitude of the tensile stresswave needed to cause fracture is significantly greater than the static tensile strength of the rock. Considering that cracks can propagate only very short distances during transit of the tensile stresswave, the higher dynamic strength can be explained quantitatively by the requirement that fracture occurs essentially simultaneously at a multitude of nucleation centers across the rock face. For wet rock, there also is evidence that heating of the water in the rock interstices by both direct electron beam heating and by thermal diffusion from the rock volume produces a thermo-hydraulic pressure which contributes to the greater spall volume observed.

Tunneling, mining and other excavation in rock are promising applications for the shock spalling technique. The prospects for technical and economic feasibility appear favorable. Some conceptual features of a Pulsed Electron Tunnel Excavator based on this technique are briefly presented.

1. INTRODUCTION

Of recent and considerable interest, are novel methods that might significantly reduce the cost and increase the speed of underground excavation and tunneling, particularly through hard rock. If successful, such methods could increase the economic feasibility of underground location of many types of facilities, such as nuclear power plants, urban transit, fuel depots, factories, inter-city high-speed railways, warehouses, and utility lines. The consequent improvement in the earth's surface environment would be readily apparent.

The technology of electron accelerators capable of pulse currents of many kiloamperes has rapidly expanded in recent years. During the design of the kiloampere ERA injector accelerator at the Lawrence Berkeley Laboratory (Ref. 1), the damage potential of the high-current electron beam was noted. This prompted the possibility of turning these effects to good use for fracturing brittle materials, particularly rock. The following two mechanisms for rock damage by electron beams were postulated (Ref. 2):

- a. Thermal crater fracturing based on quasi-static thermal stresses for subsecond pulses.
- b. Shock spalling (Ref. 3) based on intense stresses caused by submicrosecond pulses.

These are based on delivering modest amounts of energy to the rock and achieving damage by taking advantage of the low tensile strengths of brittle materials (typically 1 to 10% of

compressive strength). These techniques, as postulated, were quite different from other proposed methods of using electron or laser beams to effect rock removal by melting or vaporization (Ref. 4-8) in which very much greater amounts of energy would need to be supplied to produce the phase changes.

A study was initiated to experimentally and analytically investigate the feasibility of these mechanisms. Some preliminary results of the study were reported earlier (Ref. 9, 10). This dissertation sets forth a much more detailed presentation of the earlier findings as well as the results of more recent tests and analyses.

Analysis, discussion and results of experimental tests on the "thermal crater" fracturing technique are presented in Section 2. Similar information on the more promising "shock spalling" technique are set forth in Section 3. Prospects for the future application of the shock spalling technique to the tunneling and mining industries are briefly discussed in Section 4. Conclusions based on the studies to date are presented in Section 5.

2. "THERMAL CRATER" FRACTURING

"Thermal crater" fracturing is one of two mechanisms by which intense bursts of energetic electrons might be used to shatter rock. For reasons that will be described hereinafter, this mechanism does not appear as promising as the "shock spalling" mechanism which is discussed in Section 3.

2.1 Description and Analysis

Consider an intense burst of energetic electrons striking a rock face. As a specific example, consider the beam parameters given in Table I, although many other sets of parameters could also be considered.

As the electrons penetrate the rock, they interact strongly with the rock molecules and give up most of their energy to the lattice structure of the rock. This energy deposition appears as heat within the rock and varies with depth in the general manner shown in Figure 1. The electron range R is a measure of the density-normalized penetration depth of the electrons. The electron penetration depth varies with the accelerating potential as shown in Figure 2. Thus, for the example parameters in Table I, the penetration depth is 1.33 cm, the bombarded volume is 1.5 cm^3 and the average energy deposition is 470 J/cm^3 (112 cal/cm^3). If the rock has a density $\rho = 2.7 \text{ g/cm}^3$ and a mean specific heat $c_v = 0.2 \text{ cal/g}^\circ\text{C}$ ($0.84 \text{ kJ/kg}^\circ\text{C}$), the average temperature rise in the bombarded zone (neglecting heat transfer) is 208°C . The temperature profile versus depth is essentially the same as the energy deposition profile of Figure 1,

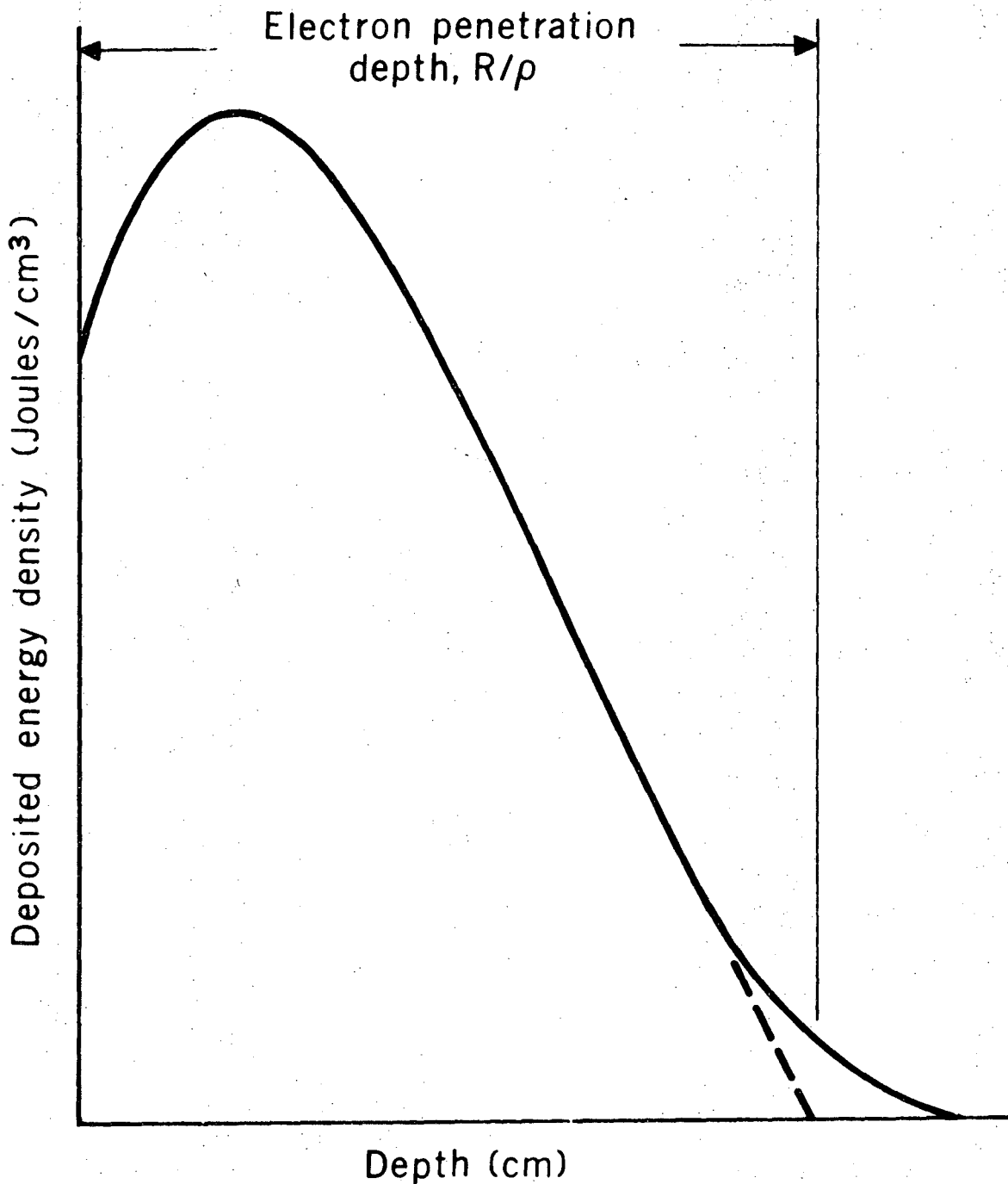
TABLE I

An example of beam parameters for thermal cratering.

Electron voltage, V	7 MV
Penetration depth, R/ρ (for $\rho = 2.7$)	1.33 cm
Beam diameter, $2a$	1.2 cm
Beam time duration, t_0	1 sec
Energy deposited, U	705 joules
Volume bombarded, $\pi a^2 R/\rho$	1.5 cm ³
Average energy deposition, $U\rho/\pi a^2 R$	470 J/cm ³ (112 cal/cm ³)

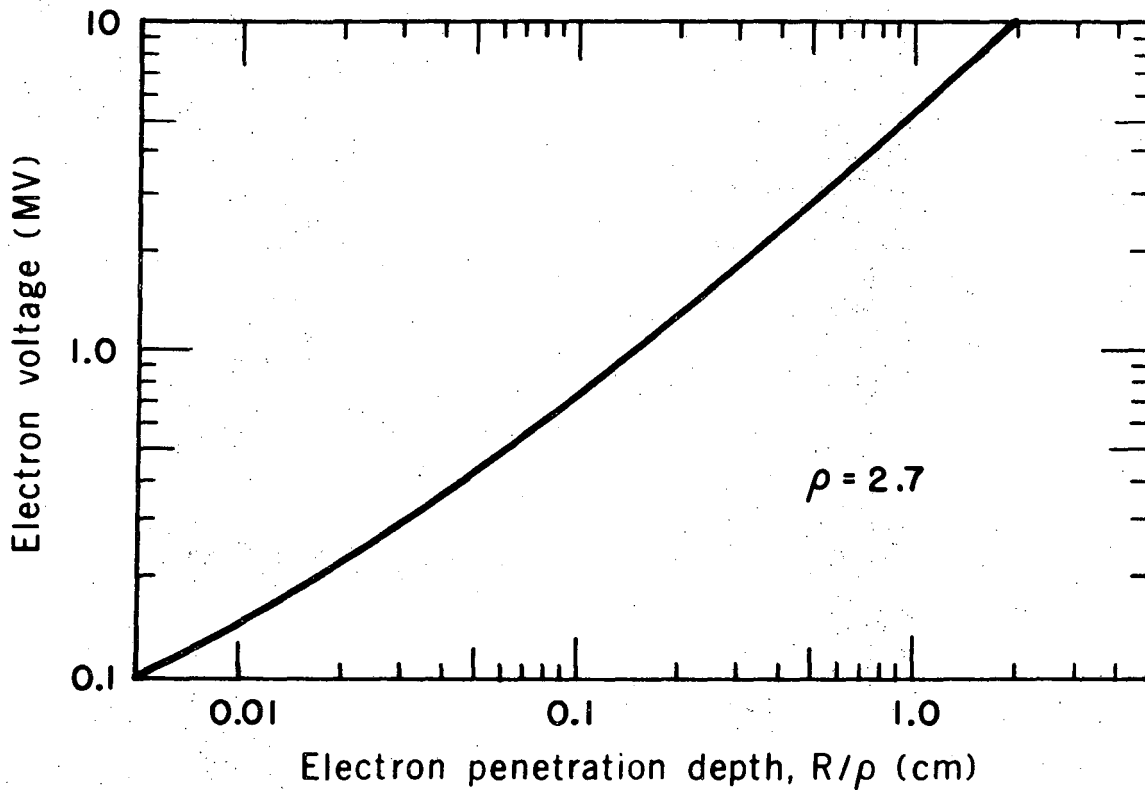
Note:

This approximates the output for one-second duration of the microwave electron linear accelerator at Building 25, Lawrence Berkeley Laboratory when operating at 120 pulses per second.



XBL 732-165

Fig. 1. Approximate distribution of energy versus depth for electron bombardment.



XBL 732-164

Fig. 2. Penetration depth versus voltage for electrons penetrating rock of 2.7 density. (Based on data for aluminum by Katz & Penfold, Rev. Mod. Phys. 24, 28 (1952))

so some spots within the bombarded zone experience less than the average temperature rise while the hottest spot experiences roughly a 50% greater than average temperature rise of $\sim 310^{\circ}\text{C}$.

After a very-short time, such a temperature rise and distribution produce significant pseudo-static thermal stresses within the rock. If a heated portion of the rock could somehow be fully restrained against thermal expansion, the associated triaxial compressive thermal stress would be

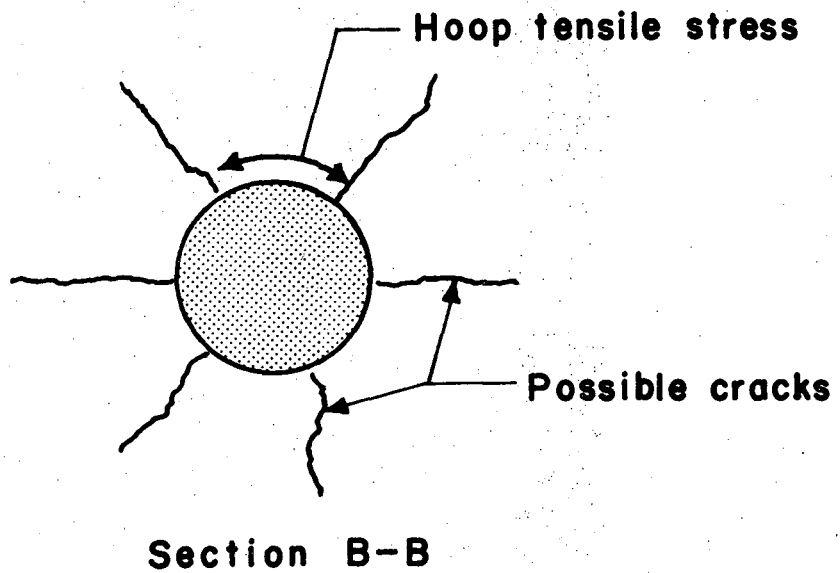
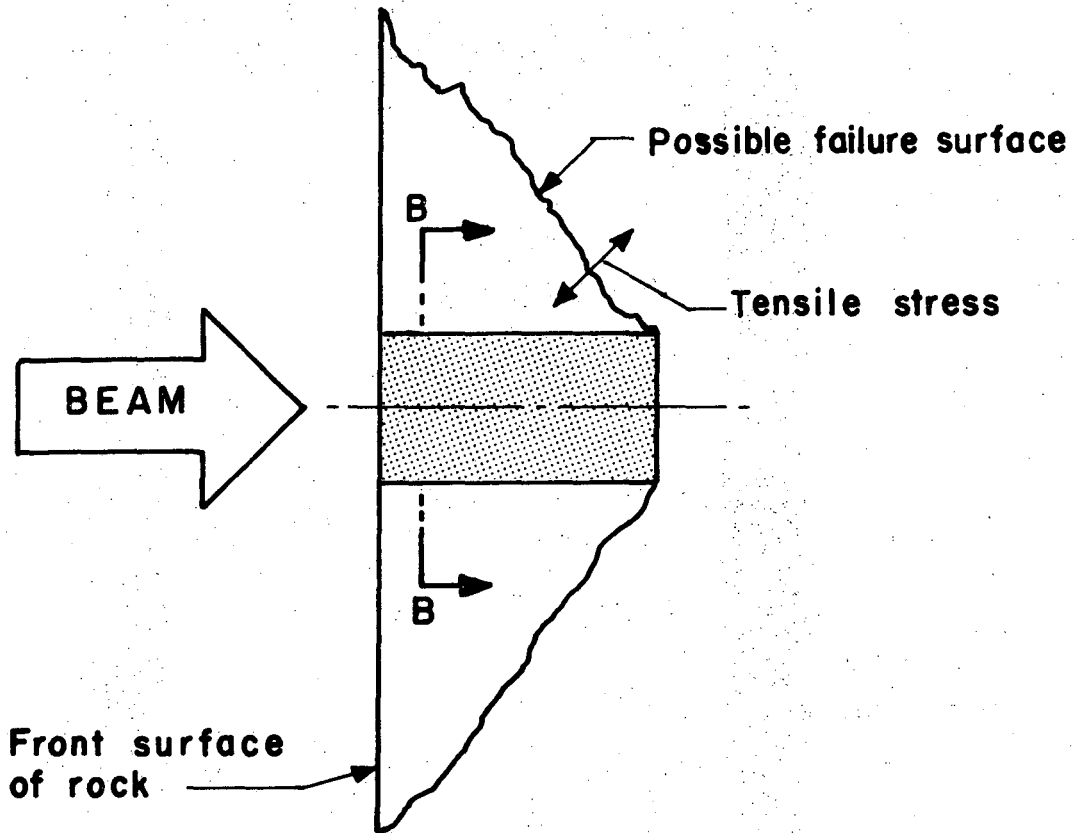
$$\sigma_o = \frac{-\alpha T_o E}{1 - 2\nu} \quad (1)$$

where α is the thermal coefficient of expansion, T_o is the initial temperature rise, E is Young's modulus of elasticity, ν is Poisson's ratio and the minus sign indicates compression. For rock with $\alpha = 8 \times 10^{-6}/^{\circ}\text{C}$, $T_o = 310^{\circ}\text{C}$, $E = 41 \text{ GN/m}^2$ ($6 \times 10^6 \text{ psi}$) and $\nu = 0.2$, the fully-restrained stress is $\sigma_o = 170 \text{ MN/m}^2$ ($25 \times 10^3 \text{ psi}$).

In reality, however, the heated portion of the rock is not fully restrained. After a short time (at least many microseconds), the stress field reaches static equilibrium with the surrounding rock mass, taking due consideration of the free surface at the rock face. Typically, the compressive stress within the heated zone is only a small fraction of σ_o . Tensile stresses are also produced in the surrounding rock, which is of particular interest since rocks typically exhibit much lower tensile strengths than compressive strengths--often only a few percent.

At the conception of this study (Ref. 11), it was postulated that the tensile stress pattern and the resultant fracture pattern might be as shown in Figure 3. As part of the early work, finite-element thermal stress computer calculations were performed (Ref. 12) to determine the magnitude and direction of the pseudo-static thermal stresses due to selected heat deposition profiles. The direction of maximum tensile stresses and a possible cracking pattern are shown qualitatively in Figure 4. The pattern is different than was postulated and does not show the hoped-for crater-shaped cracks leading to the free surface. The "computed" crack pattern is analogous to the craze pattern one might observe on a porcelain-coated metal cylinder subjected to thermal shock. This cracking pattern is such that there remains doubt that the cracked volume would break loose from the rock face. In other words, the crack pattern is not likely to result in spontaneous removal of a significant portion of the rock near the bombarded zone. However, the cracking undoubtedly would weaken the rock, so one might consider a combination of "thermal crater" fracturing plus mechanical or other removal means.

The computer calculations also gave estimates of the tensile stress magnitudes. A sample calculation for a large rock mass subjected to a peak temperature rise of 310°C indicated a maximum tensile stress of 14.8 MN/m^2 (2150 psi), which is less than 10% of the fully-restrained thermal stress σ_0 calculated earlier. Even so, this still exceeds the static



XBL 745-796

Fig. 3. Stress and fracture patterns originally postulated for "thermal crater" mode. The bombarded zone, which is in compression, is shown shaded.

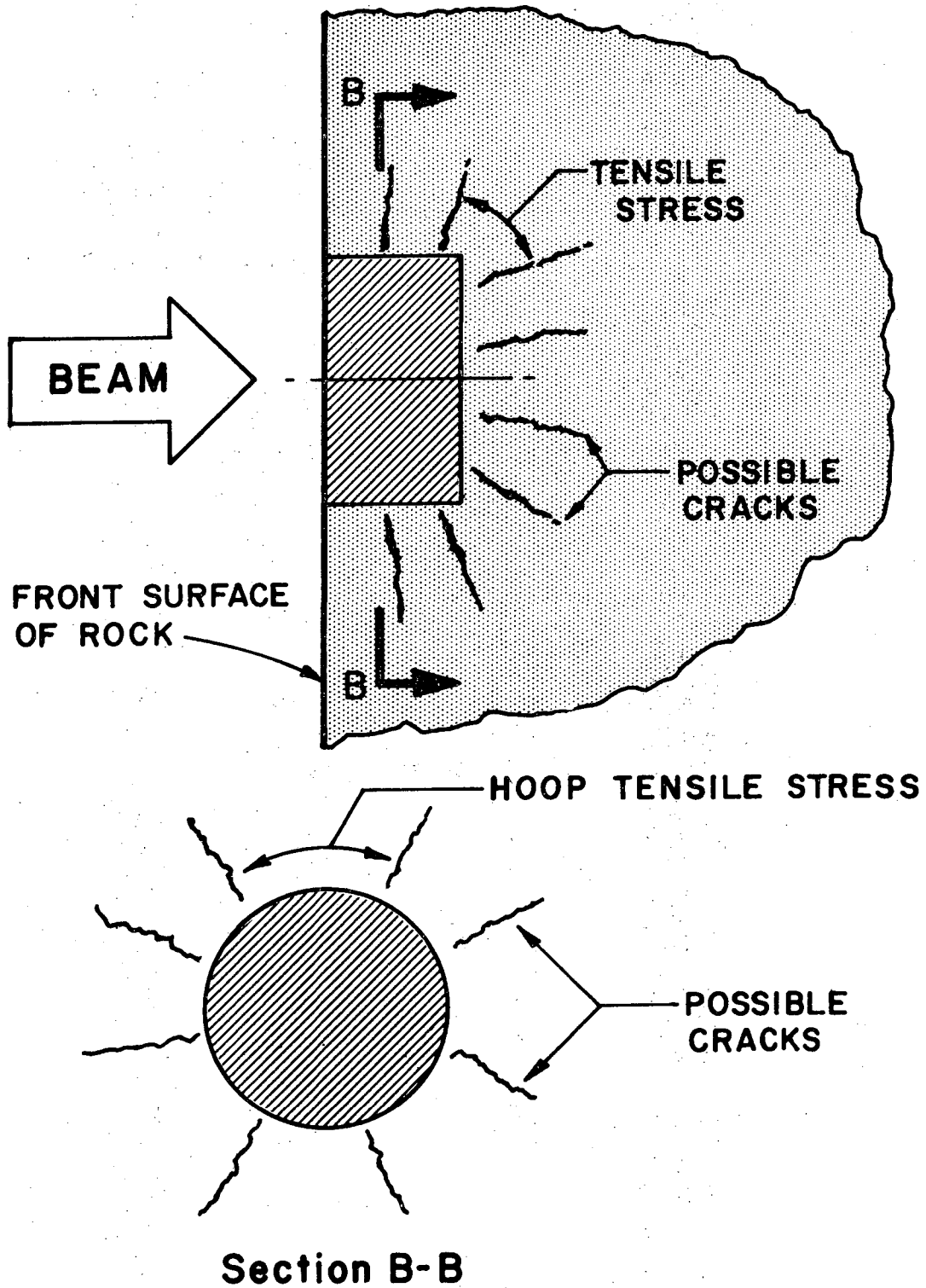
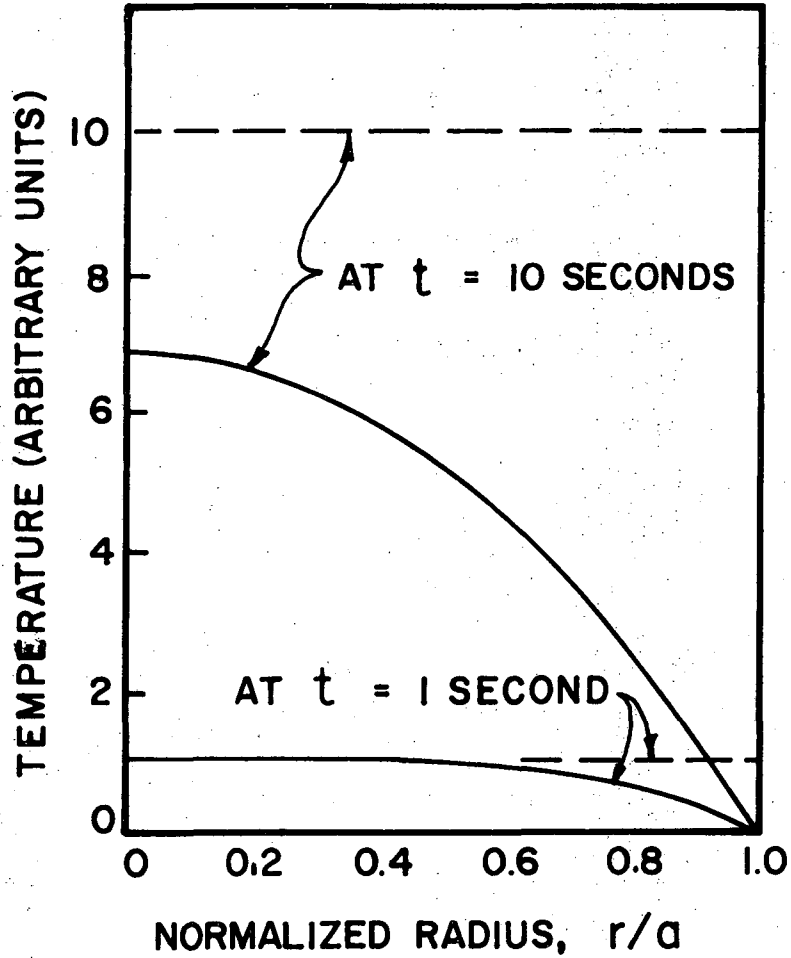


Fig. 4. Tensile stresses and likely crack patterns for "thermal crater" mode. Based on finite-element computer calculations. Bombarded zone, which is in compression, is shown shaded.

XBL 745-786

tensile strength of many rocks, and so might produce some tensile cracks in rocks so bombarded.

The question arises whether the pseudo-static assumption is valid for a one-second bombardment duration or, in contrast, whether a significant amount of heat is carried away from the bombarded volume by thermal diffusion. An exact solution would be laborious. However, an approximate answer can be obtained by considering a somewhat simplified model--namely an infinitely-long cylinder of rock with a constant internal heat production rate per unit volume per unit time after $t = 0$ and surrounded by a heat sink of infinite conductivity. This simplified case will overestimate the radial heat flow, but this error is offset to some extent by the neglect of axial heat flow. Nevertheless, it should give us a useful approximation to the actual heat diffusion conditions. Carslaw and Jaeger (Ref. 13) present a solution for this simplified case and also give a graph to simplify computations. For a thermal diffusivity $\kappa = 10^{-6} \text{ m}^2/\text{s}$ and radius $a = 0.6 \text{ cm}$, the temperature profiles after one and ten seconds are shown by solid curves in Figure 5. If there were no thermal conduction, the temperature would be as shown by the dashed lines. The effects of thermal diffusion within the rock appear modest after one second but are quite significant after ten seconds. Thus the assumption of pseudo-static thermal stresses appears reasonable for times to the order of one second or so for the case considered.



XBL 745-795

Fig. 5. Radial temperature profiles for infinite cylinder of radius $a = 0.6$ cm and thermal diffusivity $\kappa = 10^{-2}$ cm²/s subjected to uniform internal heat generation. The dashed curves apply if there is negligible heat transfer at the outer surface while the solid curves apply for a perfect heat sink at the outer surface.

2.2 Thermal Crater Experiments

To study the thermal crater-fracturing phenomenon, several rock samples were bombarded during October 1972 using the microwave-type electron linear accelerator located in Building 25 of the Lawrence Berkeley Laboratory. The approximate output characteristics of this accelerator are given in Tables I and III. Cylindrical rock samples of ~ 5 cm diameter by ~ 4 to 5 cm long were used with the electron beam striking the center of a flat face.

Observations on these tests are set forth in Table II and photos of the more interesting results are presented in Figure 6.

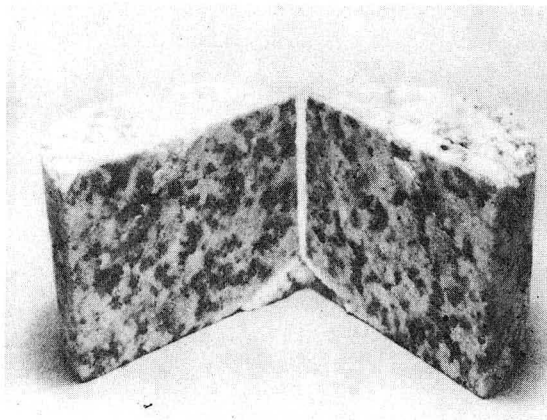
2.3 Discussion of Thermal Crater Fracturing

Bombardment for one second, as contemplated in Section 2.1, produced no apparent weakening. In fact, neither did bombardment for five seconds, in which case the peak temperatures are estimated to exceed 500 °C. When bombarded for ten seconds, some of the samples did exhibit melt "squirts" and some cracking. To achieve significant pseudo-static thermal stress cracking apparently requires peak temperatures at or approaching the melting temperature of the rock. Raising the rock temperature so high requires a large energy input, which opens to question the economic practicality of such long (1 to 10 second) bursts as a primary excavation method. The observed results of melting, plus possible cracking, after large inputs of energy are quite similar to the results reported by

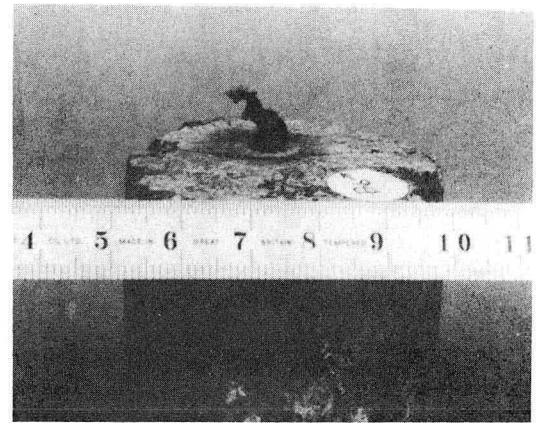
TABLE II
Thermal cratering test observations.

Samples bombarded by 7 MV electron linear accelerator at Building 25, LBL.

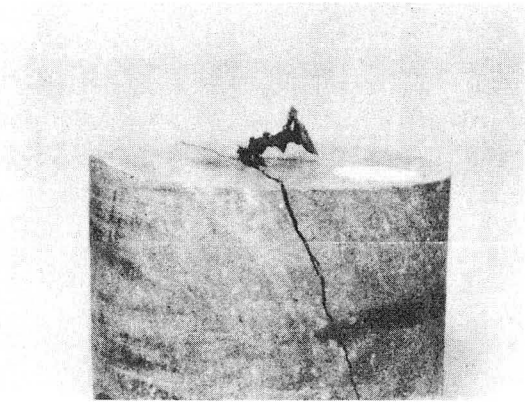
Test No.	Rock type	Bombard duration (seconds)	Observations
B1	Coarse Sandstone	0.5	No visible effect.
B2	Coarse Sandstone	1	Dark spot a few mm diameter. No apparent weakening.
B3 } B4 }	Coarse Grano-diorite	~ 2 each	Discolored. No apparent weakening, even when sectioned through bombarded spot.
B5	Coarse Grano-diorite	10	Discolored region ~ 1.5 cm diameter. No spalling. Later inspection revealed some cracks.
B6	Schist	9	Discolored. Some melting with "lava" squirting out.
B7	Greenstone	5	Discolored spot. No apparent weakening.
B8	Greenstone	10	Discolored spot. Radial cracks. Some melting with "lava" squirting out.
B9	Fine Sandstone	5	Discolored spot. No apparent weakening.
B10	Fine Sandstone	10	Discolored spot with central portion slightly raised. No cracks or evident weakening. When observed several seconds after bombardment, the central spot was observed to be still bright red.
B11	Fine Grano-diorite	5	Discolored spot. No apparent weakening.
B12	Fine Grano-diorite	10	Discolored spot. Some hairline cracks.



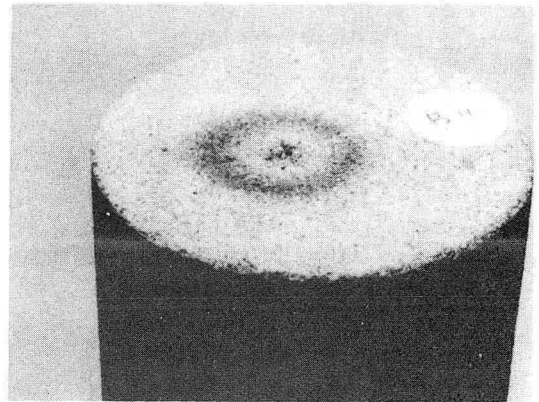
a



b



c



d

XBB 744-2845

Fig. 6. Photos of rock samples exposed to "thermal crater" mode of electron bombardment for approximately 10 seconds. a) Test B5: Coarse grano-diorite sectioned after bombardment to show small cracks, b) Test B6: Schist, c) Test B8: Greenstone, and d) Test B10: Fine sandstone.

Schumacher et. al. (Refs. 5-7) for continuous unpulsed electron beams. It appears from these preliminary tests that the "thermal crater" fracturing mechanism offers little, if any, commercial advantages over the earlier electron-beam techniques, so subsequent program efforts were directed solely to the more promising "shock spalling" technique.

TABLE III

Typical operating parameters of electron accelerators during rock bombardment experiments.

Test dates	Accelerator used	Location	Beam voltage E (MV)		Calc. max. penetration depth for $\rho=2.7$ h (cm)	Approx. beam diameter D (cm)	Approx. bombarded volume $V=\frac{\pi}{4}D^2h$ (cm ³)	Pulse rep rate f (Hz)	Pulse duration t (10 ⁻⁹ s)	Pulse current, mean \bar{I} (kA)	Energy delivered $U = \bar{E} \bar{I} t$ (J)	Per pulse		Remarks
			Mean	Max								Typical central energy fluence $u_0 = 4U/\pi D^2$ (kJ/cm ²)	Typical central electron fluence $q = u_0/E$ ($\mu\text{C}/\text{cm}^2$)	
May 1971	Febetron 705	LLL Bldg. 255	1.4	2.2	0.39	1.7	0.8	Single pulse	100	2.0	2.8×10^2	0.13	93	Values at 0.6 cm from accelerator output window.
Oct 1972	Microwave Electron Linac	LBL Bldg. 25	~ 7	~ 7	1.33	1.2	1.5	up to 120	6000	1.4×10^{-4}	5.9	0.005	0.7	Values at 1 cm from accelerator output window.
Dec 1972	Astron Linac	LLL Bldg. 431	5.8	5.8	1.10	~1.0	~0.9	1	300	0.3	5.2×10^2	~0.66	~114	Values at 0.7 cm from accelerator output window.
Jan 1973	Febetron 705	LLL Bldg. 341	1.2	1.9	0.33	1.6	0.7	Single pulse	100	1.6	1.9×10^2	0.09	75	Values at 0.6 cm from accelerator output window.
Feb 1973	Pulserad 422 (co-axial mode)	LLL Bldg. 169	1.0	1.3	0.22	4.8 (3.1)	4.0 (1.7)	Single pulse	80	39	3.1×10^3	0.17 (0.40)	170 (400)	Values at 5 cm (parenthetical values at 2.5 cm) from accel. output window.
Mar 1973	Pulserad 422 (co-axial mode)	LLL Bldg. 169	1.1	1.4	0.24	6.3 (3.8)	7.4 (2.8)	Single pulse	90	37	3.7×10^3	0.12 (0.32)	110 (290)	Values at 5 cm (parenthetical values at 2.5 cm) from accel. output window.
Aug 1973	Pulserad 422 (triaxial mode)	LLL Bldg. 169	2.0	3.1	0.57	3.6	5.9	Single pulse	70	22	3.1×10^3	0.30	150	Values at 5 cm from accel. output window.
Nov 1973	Pulserad 1140	Physics Intl. Co. San Leandro	~ 4.0	~ 5.0	0.94	3.5	9.1	Single pulse	100	24	9.5×10^3	0.96	320	Values at 3 cm from window on partial atmosphere chamber.
Jan 1974	Hermes II	Sandia Corp. Albuquerque	~ 9	12.5	2.41	9.0	221	Single pulse	160	45	6.4×10^4	1.00	78	Values at 18 cm from accelerator output window.

Notes:

1. To convert joules to calories, multiply given value by 0.239.
2. Fluence values given are on axis and are typical of conditions used for actual tests.
3. Approximate beam diameter calculated such that beam area = energy delivered/central energy fluence. Some of the electron beam falls outside of the beam diameter so calculated.

3. "SHOCK SPALLING" TECHNIQUE

3.1 Description

The "shock spalling" technique also uses an intense burst of energetic electrons to achieve rock fracturing. The major distinction from the thermal crater technique previously discussed is that the burst is very intense and of very short duration--typically less than one microsecond. The bombardment of the rock is of such short duration that stresswaves do not travel any significant distance during bombardment. In practice, the bombardment can be considered almost instantaneous. Further explanation of the mechanisms of shock spalling is deferred until Section 3.3 in the belief that they can be better appreciated after a presentation of the experimental observations on the shock spalling process.

3.2 Shock Spalling Experiments

Experimental bombardments using intense bursts of energetic electrons have been carried out on a variety of rocks using the different electron accelerators set forth in Table III. The electron linear accelerator used for the thermal crater experiments described earlier is also listed for comparison. These accelerators had already been constructed for other purposes and were not specifically designed for rock spalling. Nevertheless, a limited range of tests was possible using these machines.

Almost all bombardment tests since November 1972 have been performed on the five rock types listed in Table IV which

TABLE IV
Summary of measured properties of selected rock types.

	Rock group	Igneous		Sedimentary		Metamorphic
	Rock type	Sierra Granite	Napa Basalt	Lyons Sandstone	Limestone (Marble)	Greenstone (Amphibolite)
Density (gm/cm ³)		2.65	2.87	2.66	2.73	2.91
Thermal Coefficient of Expansion (10 ⁻⁶ /°C)		7.00	5.60	11.30	5.20	7.00
Modulus of Elasticity (10 ³ ksi) (10 ⁹ N/m ²)*		7.80 54.	10.40 72.	1.90 13.1	6.00 41.	14.30 99.
Poisson's Ratio		0.18	0.21	0.23	0.30	0.28
Compressive Strength (ksi) (10 ⁶ N/m ²)*		25.60 177.	46.20 319.	6.21 42.9	8.43 58.1	39.60 273.
Porosity (void volume/total volume)		0.0088	0.0048	0.1780	0.0085	0.0022

*Newtons per square meter

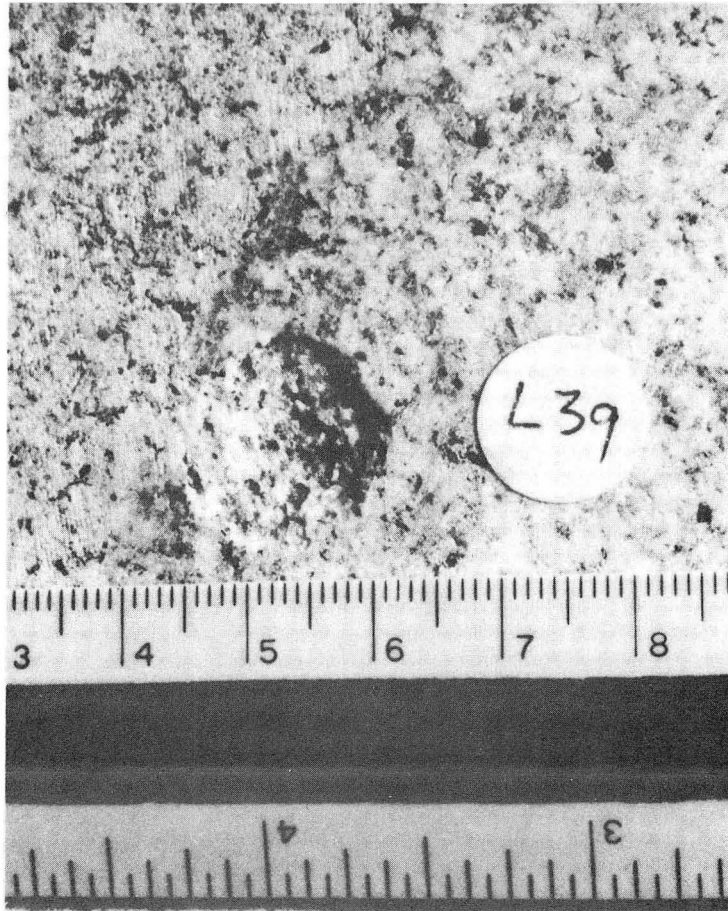
were selected to cover a range of hardness, compressive strength, and porosity, as well as representing the igneous, metamorphic and sedimentary groups of rock. Some of the properties of these five rock types were determined (Ref. 14) and are presented in Table IV.

The results of the shock spalling bombardment tests are summarized in the following subsections.

3.2.1 Febetron Tests. The earliest tests using the Febetron #705 pulsed electron accelerator were conducted in May 1971. These tests resulted in successful shock spalling which was reported previously (Ref. 11). The spalls were of modest size (up to 16 mm diameter x 0.9 mm deep for wet granite and 18 mm diameter x 1.2 mm for wet sandstone), but the energy input was also modest (~ 280 joules).

Further tests using a different Febetron #705 accelerator were performed in January 1973. The shock spalling mechanism was reconfirmed. Spalls up to 15 mm diameter by 1.2 mm deep were obtained in wet granite, shown in Figure 7, which is comparable to the earlier results. An interesting result of this series of tests was that dry granite blocks would not spall, while under like conditions wet granite blocks would spall. It was obvious that water enhanced the spalling mechanism, but the exact means of enhancement were not clear at that time. This effect will be discussed in more detail later.

3.2.2 Tests at Astron. It was of interest to study the effect of rapid repetitive bursts of energetic electrons. The residual cracking or residual heat from earlier pulses could



XBB 744-2846

Fig. 7. Wet Sierra granite block bombarded in air with single shot (1.9 MV, 0.19 kJ, 100 ns) from Febetron #705 electron accelerator.

possibly enhance spalling on subsequent pulses. Most accelerators capable of producing the very-short-duration bursts required for shock spalling only deliver a single burst with a turn-around time of at least a few minutes, presumably because rapid pulsing was considered not important. An exception is the Astron linear accelerator (Ref. 15, also see Table III) which is located at the Lawrence Livermore Laboratory. It is capable of operating continuously at a repetition rate of one to several pulses per second and is capable also of delivering a rapid sequence of at least one hundred pulses at the rate of one thousand pulses per second. The energy delivered per pulse is somewhat greater than that of the Febetron and led to the hope that the Astron linear accelerator would produce shock spalling.

Tests were performed at the Astron linear accelerator during December 1972. A pneumatic plunging mechanism and controls were constructed which, during the one-second interval between pulses, could plunge the rock sample into the beam path, leave it there for a preselected one or more pulses, and then withdraw the rock prior to the next following pulse. Several different rock types, including wet granite and wet sandstone, were subjected to a single pulse of this beam but no spalls were produced. This was in spite of the fact that the electron fluence (time-integrated beam current density) through the rock (see Table III) was believed to be greater than for the Febetron #705 which had successfully produced shock spalling. It is suspected that the lack of successful spalling was either due to the fluence being lower than calculated (e.g. lower current or

larger beam size) or due to the penetration depth of the Astron beam being several times greater than for the Febetron thereby propagating stresswave energy in the radial direction as well as in the axial direction.

Discussions with the Astron staff have indicated that improved performance from the Astron accelerator is possible, but is time-consuming and therefore expensive. It is not known whether such improved performance definitely will produce spalling. Consequently, the main thrust of the experimental program was directed to the tests described below which appeared more certain of producing significant spalling.

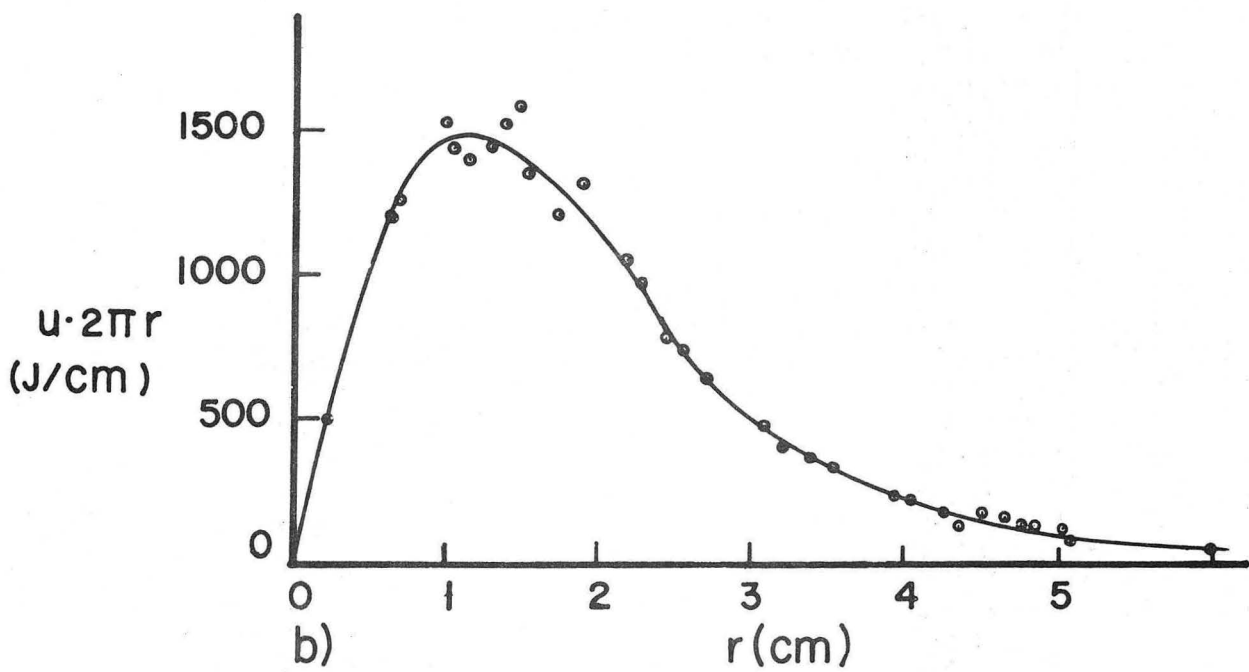
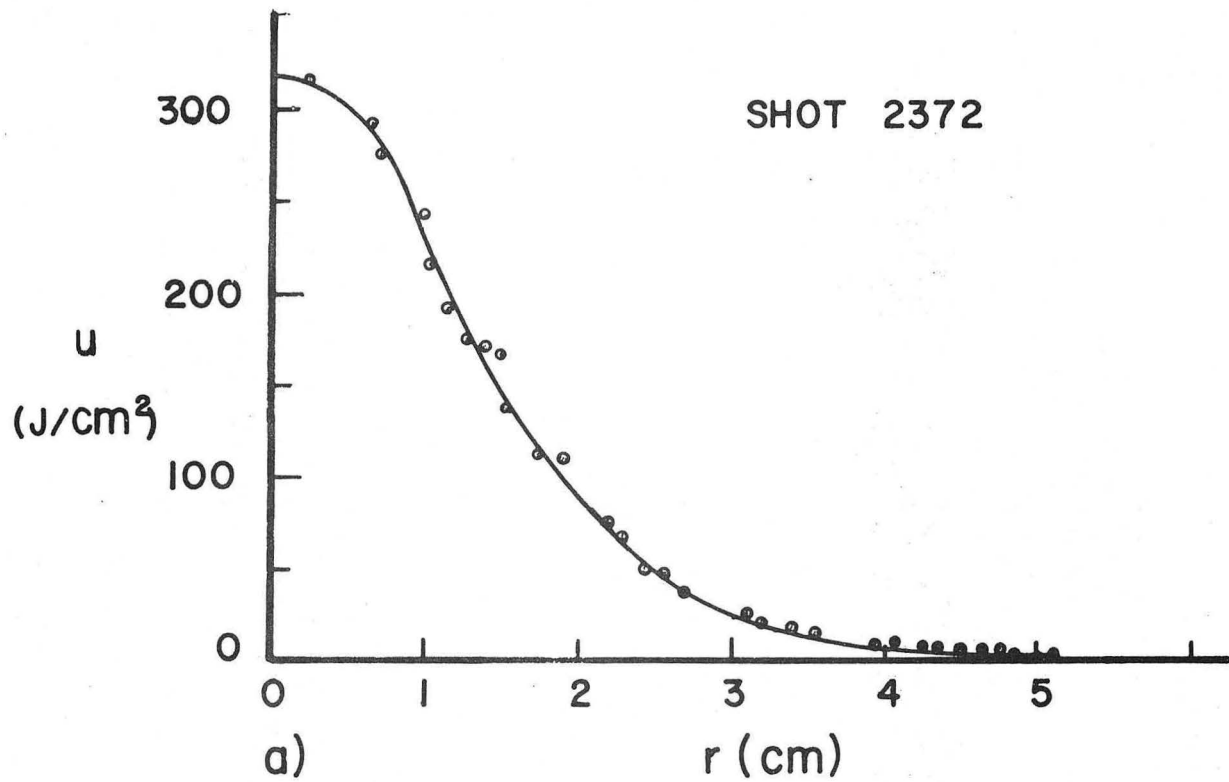
3.2.3 Tests Using Pulserad 422 Accelerator

The Pulserad 422 electron accelerator (manufactured by Physics International Company, San Leandro, California) located at the Lawrence Livermore Laboratory was used for three series of rock bombardment tests--one each during February, March and August 1973. During the first two tests the accelerator was connected in its "coaxial" mode with a mean output voltage of 1.0 to 1.1 MV, while for the third test it was connected in its "triaxial" mode which produces a mean output voltage of ~ 2.0 MV. The output characteristics for both modes are included in Table III.

This accelerator facility had good beam diagnostics equipment including fast oscilloscopes to view voltage and current waveforms during the short duration pulse. The energy delivered over the bombarded surface was determined using a segmented carbon calorimeter made up of an array of small

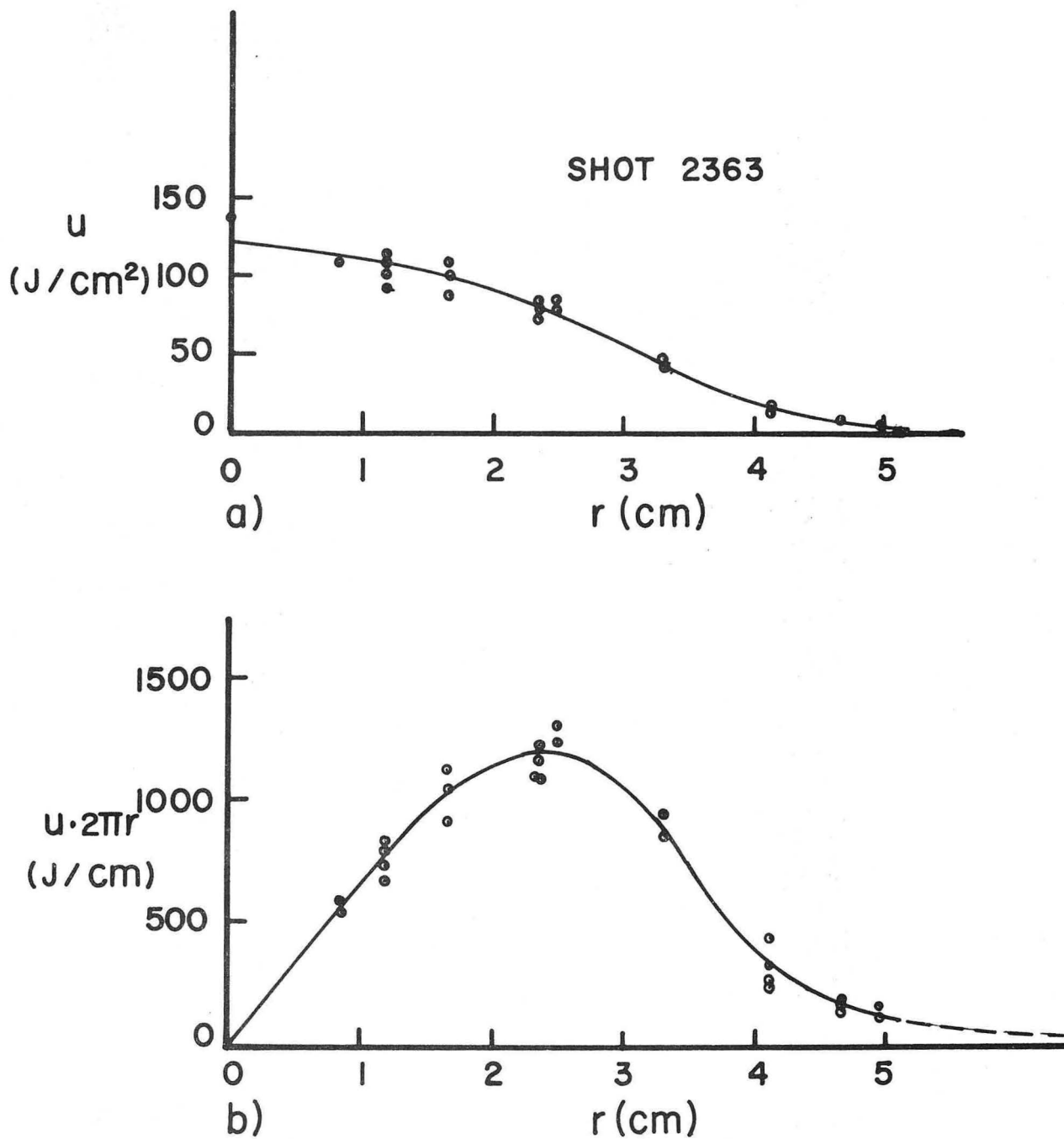
carbon blocks, each having its own thermocouple. Fast digital printout allowed the temperature rise and the corresponding energy input to each block to be determined. Typical curves showing the measured energy fluence u at the calorimeter as a function of radius r from the beam centerline are shown in the upper curves of Figures 8 and 9 for the tests conducted in March 1973. The calorimeter was spaced from the accelerator output window at the "standoff distance" identified on each figure. Inspection shows a bell shaped distribution which is roughly Gaussian. The lower curves in Figures 8 and 9 show $u(2\pi r)$, which is the energy deposited per unit increment of radius, as a function of radius r . The area under this latter curve out to any given radius represents the amount of energy deposited within that radius. By extrapolating the curve (shown dashed) to large radii, the total energy deposited $U = \int u(2\pi r) dr$ was estimated. These estimates agreed closely with separate estimates based on the voltage and current waveforms previously mentioned.

The general arrangement for bombarding the rocks is shown diagrammatically in Figure 10. Most of the tests were conducted at a standoff distance (distance beam travels in air from accelerator output window to the rock or calorimeter) of 2.5 cm or 5.0 cm, but a few successful tests were conducted at distances up to 15 cm during the August 1973 tests. Tests were conducted on wet and dry samples of the five rock types previously described, with shock spalling achieved for all types, both wet and dry. A wet white limestone block subjected to a



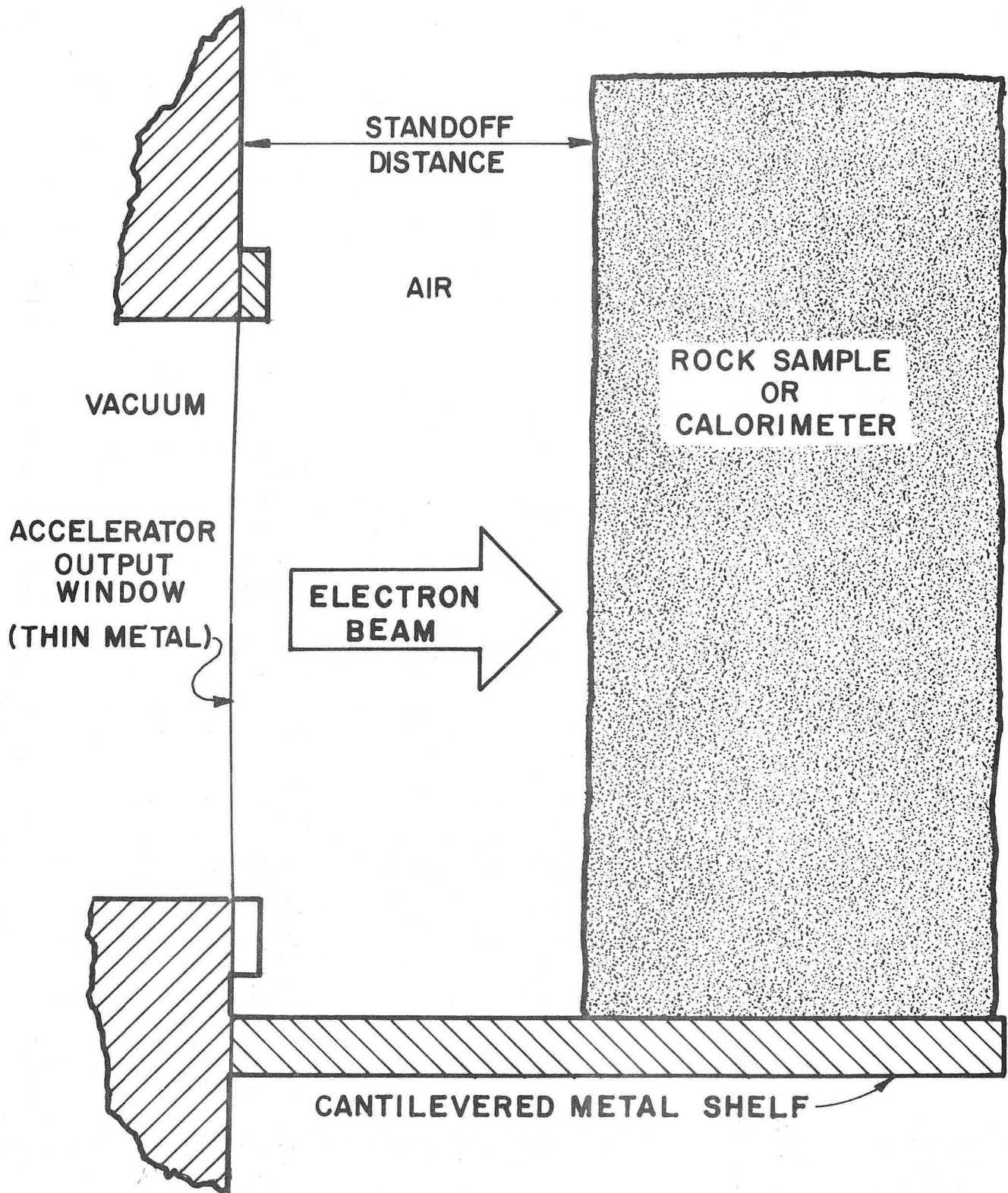
XBL 745-794

Fig. 8. Typical energy fluence at 2.5 cm from output window of Pulserad 422 electron accelerator expressed a) in joules per square centimeter of surface and b) in joules per centimeter of radius.



XBL 745-793

Fig. 9. Typical energy fluence at 5 cm from output window of Pulserad 422 electron accelerator. Energy fluence expressed a) in joules per square centimeter of surface and b) in joules per centimeter of radius.



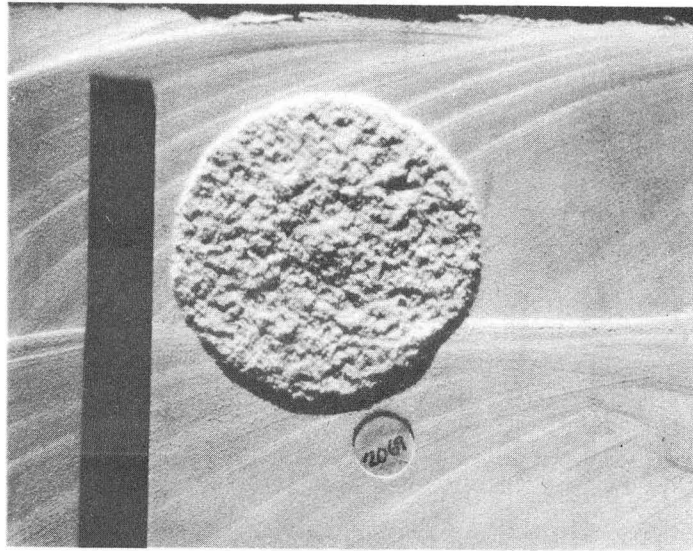
XBL 745-792

Fig. 10. Experimental arrangement for shock spalling tests at Pulserad 422 electron accelerator.

single shot is shown in Figure 11 together with the sandy debris produced. A wet granite slab subjected to two almost-overlapping "shots" is shown in Figure 12 together with the sandy debris produced. Shot #2390 removed ~ 20% more rock than Shot #2389, possibly indicating that the earlier shot enhanced the spall volume on the second shot. A wet slab of hard basalt subjected to two shots at the same spot and the associated debris are shown in Figure 13. Compared to Shot #2393, the earlier Shot #2392 produced a spall ~ two-thirds as large--the approximate outline of which can be seen within the later spall. This again possibly indicates spall enhancement on subsequent shots. A strong wet greenstone block subjected to a single shot is shown in Figure 14 together with the somewhat flaky debris therefrom.

Shot #2071 was a particularly interesting one in which a 1.0 cm thick slab of wet granite was located in air at 2.5 cm from the output window of the Pulserad 422 and also subjected to a single pulse. Spalling occurred at both front and rear faces as shown in Figure 15. Figure 16 presents several frames from a high-speed movie which shows the rather violent spalling at the front surface facing the accelerator and a slower, flake-like spalling at the rear face. Since the rock is ~ 5 electron ranges thick, the rear spall appears clearly to be due to a traveling stresswave unassisted by other phenomena such as thermal or electric charge effects.

Another series of tests were performed in August 1973, again using the Pulserad 422 accelerator, but with mean acceleration potential of ~ 2.0 MV instead of the ~ 1.0 MV



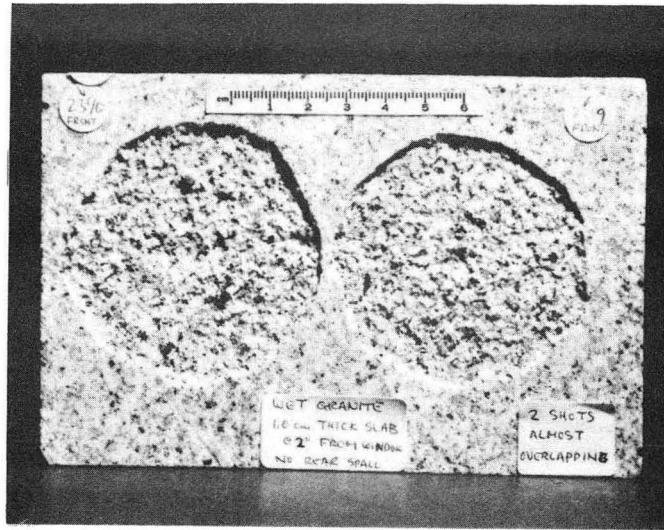
a



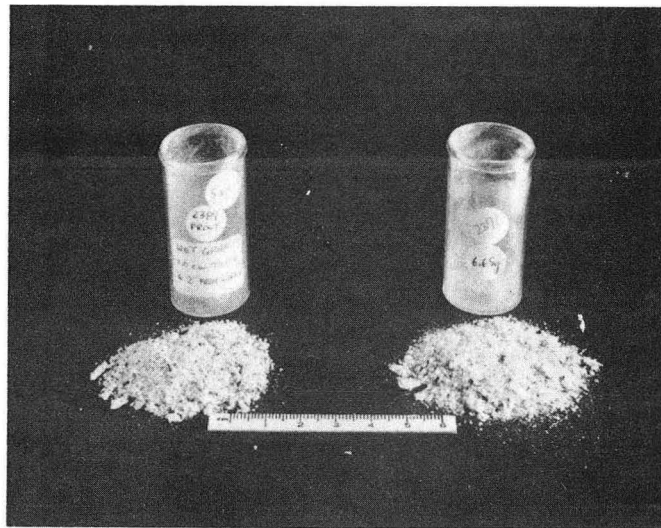
b

XBB 744-2850

Fig. 11. a) Wet white limestone block 10 cm thick bombarded in air with single shot (1.3 MV, 3.1 kJ, 80 ns) from Pulserad 422 electron accelerator. b) The spall debris therefrom.



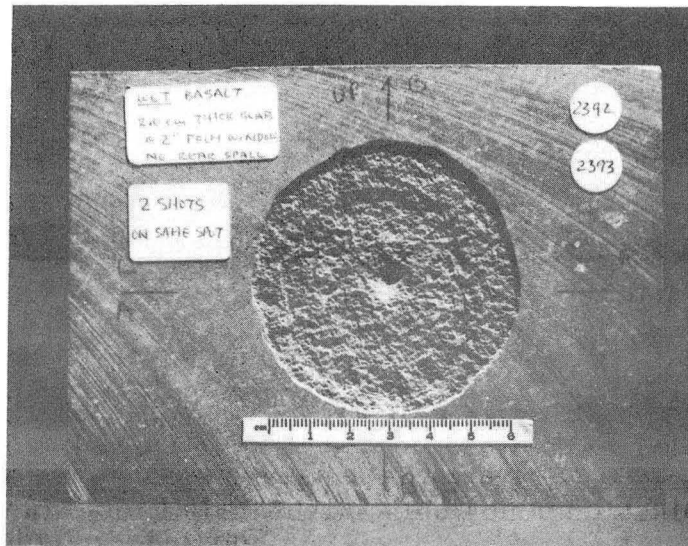
a



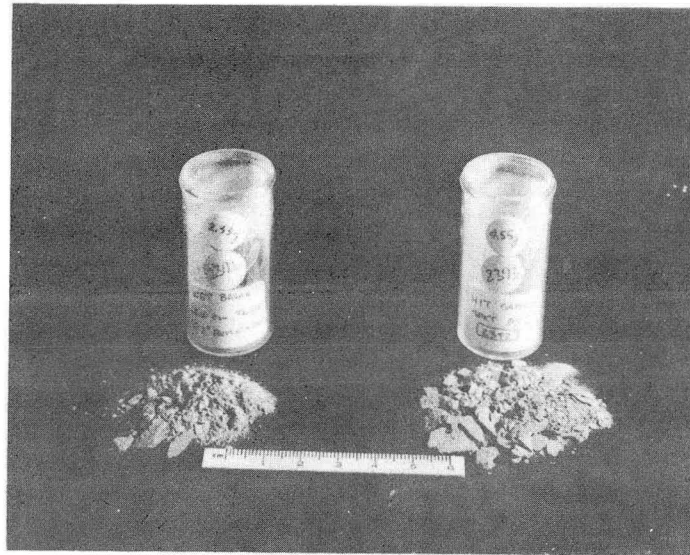
b

XBB 744-2848

Fig. 12. a) Wet Sierra granite slab 1 cm thick bombarded in air with two separate shots (1.4 MV, 3.7 kJ, 90 ns) from Pulse-rad 422 electron accelerator. b) The spall debris therefrom.



a



b

XBB 744-2848

Fig. 13. a) Wet Napa basalt slab 2 cm thick bombarded in air with two space-coincident but time-spaced shots (1.4 MV, 3.7 kJ, 90 ns) from Pulserad 422 electron accelerator. b) The spall debris therefrom.



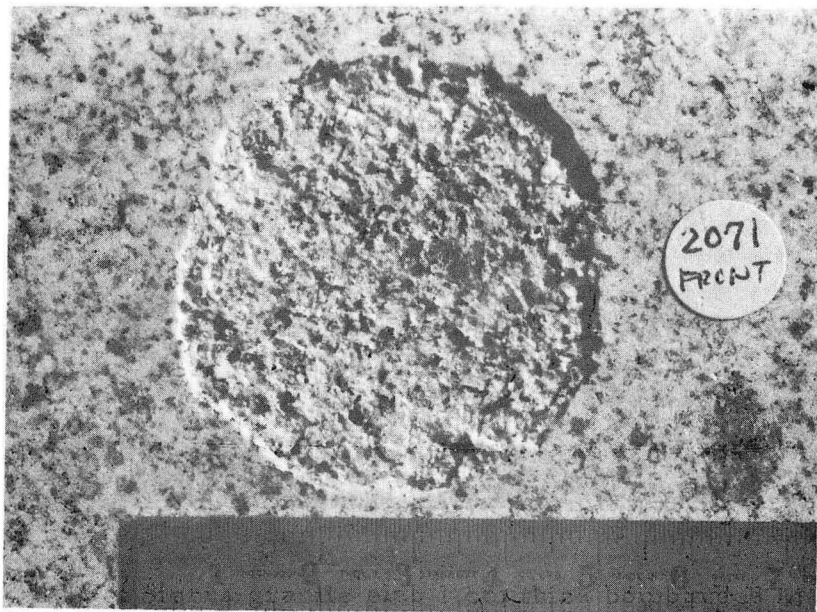
a



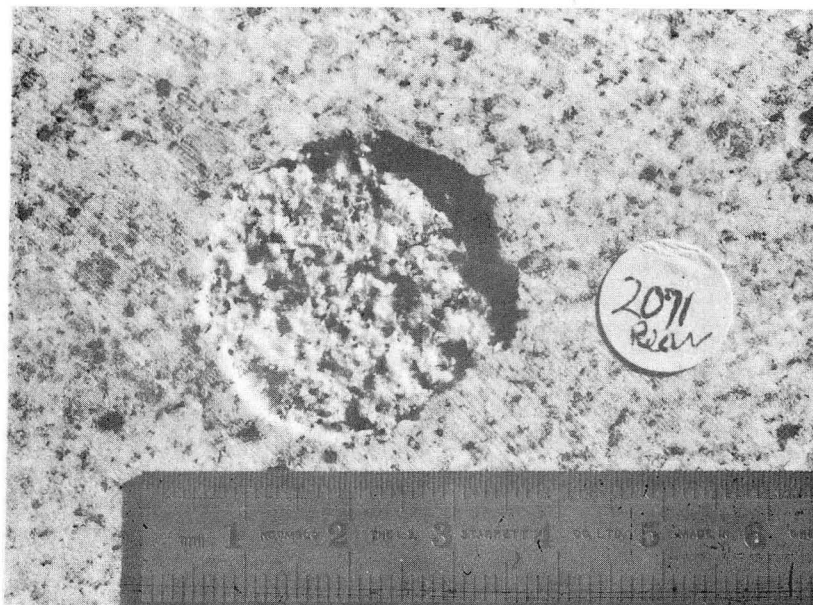
b

XBB 744-2849

Fig. 14. a) Wet greenstone block 10 cm thick bombarded in air with single electron shot (1.4 MV, 3.7 kJ, 90 ns) from Pulserad 422 electron accelerator. b) The spall debris therefrom.



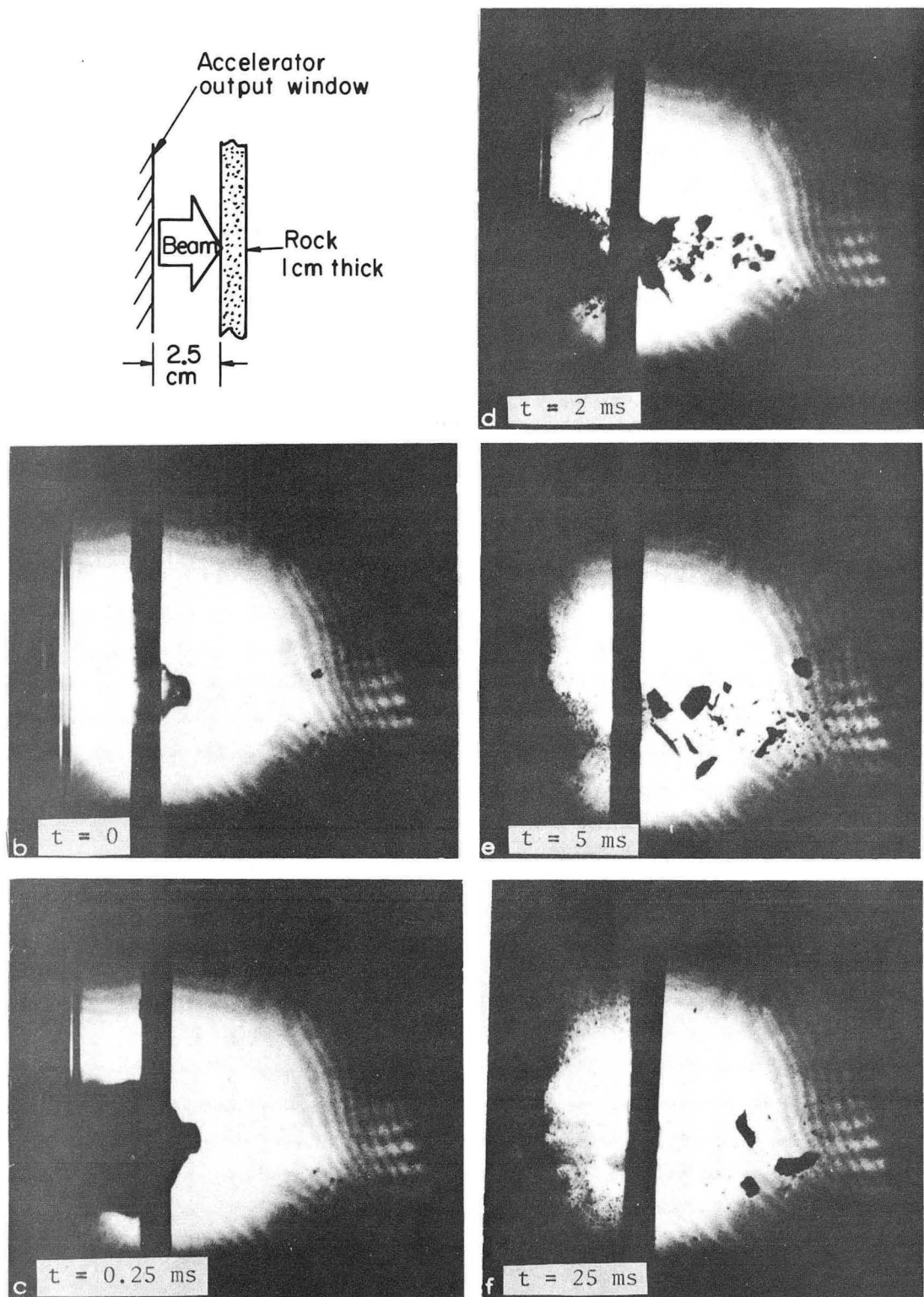
a



b

XBB 744-2856

Fig. 15. Wet Sierra granite slab 1 cm thick bombarded in air with single electron shot (1.3 MV, 3.1 kJ, 80 ns) at 2.5 cm from Pulserad 422 electron accelerator. a) Spall on front surface and b) spall on rear surface due to stresswave traveling through slab.



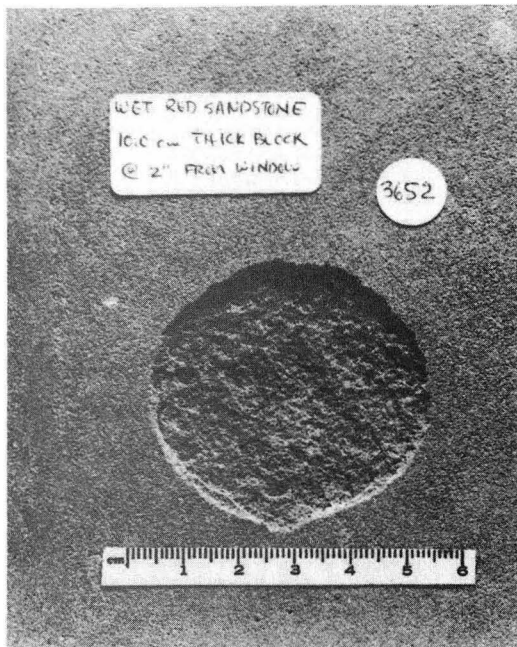
XBB 745-2976

Fig. 16. Frames from high-speed movie showing spalling at both front and rear surfaces of rock in previous figure. Note that front spall is sandy and rapid while rear spall is flaky and slower.

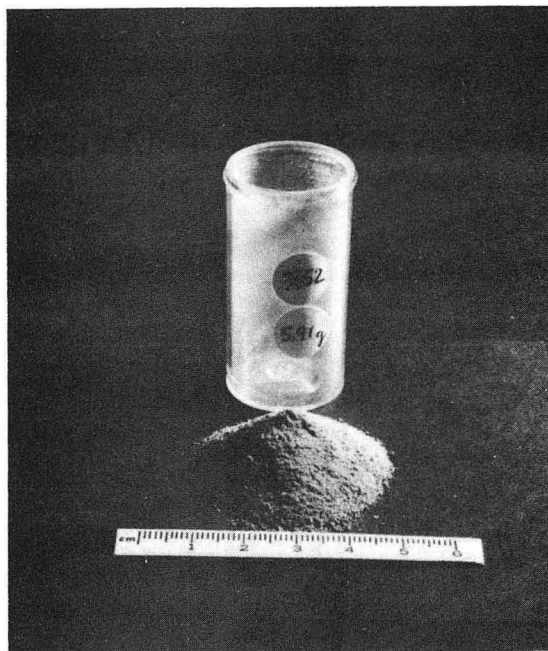
of the earlier tests. The energy delivered per shot was 3 to 4 kJ as for the earlier tests. At the higher voltage, the electrons penetrated more deeply into the rock and consequently produced a deeper spall. Successful spalling was achieved at various standoff distances up to 0.15 meter from the accelerator exit port.

Successful shock spalling of hard rocks having been demonstrated, it was of interest whether it also would work on softer materials. A wet weak sandstone block bombarded with a single shot produced the spall and the sandy debris shown in Figure 17. Single-shot bombardment of a wet shale produced the spall shown in Figure 18. The debris was a fine dusty powder. Some frames from a very-high-speed movie of this bombardment of wet shale are exhibited in Figure 19 and show definite spall movement at the first frame ($5 \mu\text{s}$) after bombardment and indicate a maximum spall velocity of 580 m/s (1300 miles/hour). Single-shot bombardment of a moist plastic adobe clay produced the spall shown in Figure 20.

Data on the foregoing bombardments are presented in Table V. The spall diameter corresponds to a circle with area equal to that measured for the spall. The spall depth was measured with a depth micrometer. The spall volume was measured by filling the recess with fine alumina powder of known bulk density. Specific energy was calculated as the quotient of total energy deposited divided by the volume removed. Specific energy is nearly constant for a given rock material and excavation method, independent of scale, and can



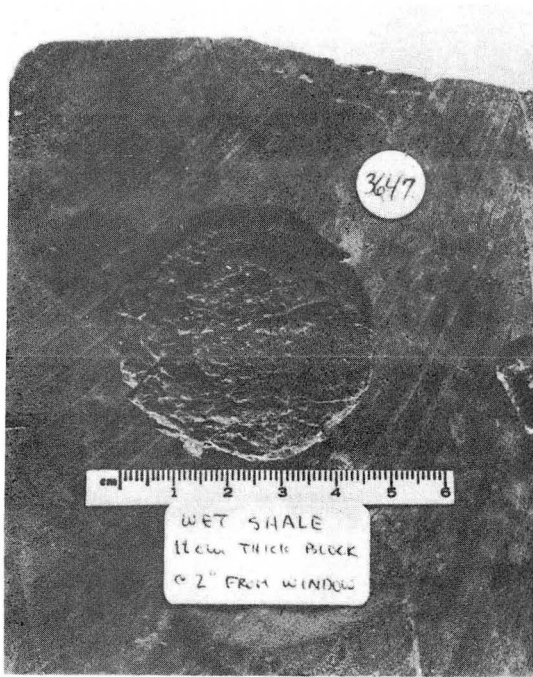
a



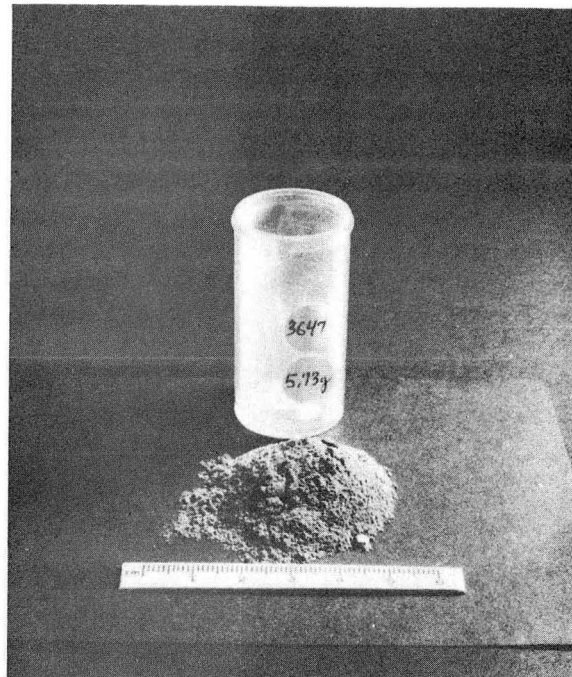
b

XBB 744-2847

Fig. 17. a) Wet Lyons sandstone block 10 cm thick bombarded with single shot (3.1 MV, 3.1 kJ, 70 ns) from Pulserad 422 electron accelerator. b) The spall debris therefrom.



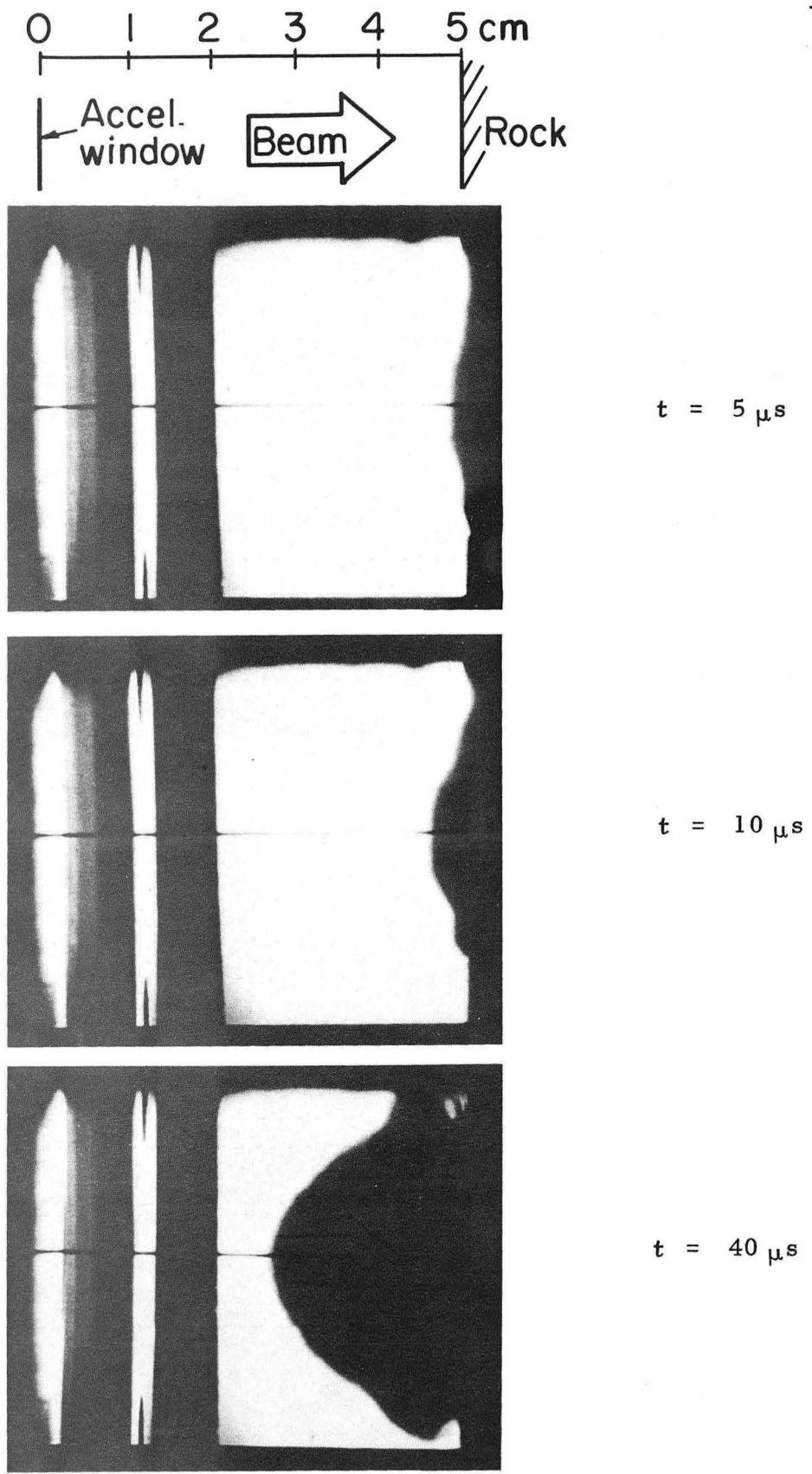
a



b

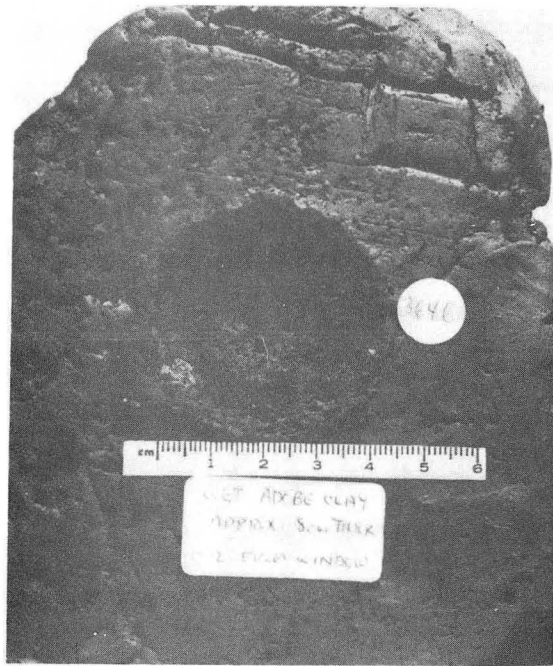
XBB 744-2854

Fig. 18. a) Wet shale block 11 cm thick subjected to a single shot (3.1 MV, 3.1 kJ, 70 ns) from Pulserad 422 electron accelerator. b) The spall debris therefrom.

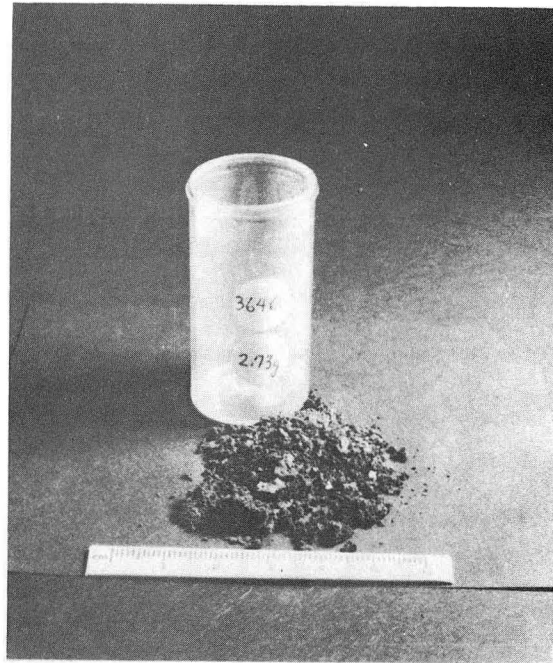


XBB 745-2977

Fig. 19. Selected frames from very-high-speed movies of Shot 3647 onto wet shale. Maximum spall velocity is 580 meters per second (1300 miles per hour).



a



b

XBB 744-2853

Fig. 20. a) Moist adobe clay ~ 8 cm thick subjected to a single shot (3.1 MV, 3.1 kJ, 70 ns) from Pulserad 422 electron accelerator. b) The spall debris therefrom.

TABLE V

Single-shot spall data for several tests using Pulserad 422 Accelerator.

		Moist Adobe Clay	Colorado Red Sandstone	Shale	White Limestone (Marble)	Sierra Granite	Napa Basalt	Green- stone
Compressive strength	MN/m ² ksi	Not meas.	43 6	Not meas.	58 8	180 26	320 46	270 40
Young's modulus of elasticity	GN/m ² 10 ⁶ psi	Not meas.	13 1.9	Not meas.	41 6	54 8	72 10	99 14
Shot Ident. No.		3646	3652	3647	2069	2390	3634	2373
Date		8/73	8/73	8/73	2/73	3/73	8/73	3/73
Mean accelerating voltage	MV	2	2	2	1.0	1.1	2	1.1
Standoff distance	cm	5	5	5	5	5	5	2.5
Total energy deposited	kJ	3.1	3.1	3.1	3.1	3.7	3.1	3.7
Spall diameter	cm	4.5	5.0	4.7	6.6	6.7	4.4	3.8
Spall area	cm ²	16	20	17	34	35	15	11
Spall depth, max	cm	1.0	0.26	0.29	0.08	0.13	0.19	0.13
Volume removed	cm ³	6.8	3.4	3.2	2.6	3.1	1.8	1.0
Specific energy (energy deposited/volume removed)	kJ/cm ³	0.46	0.9	1.0	1.2	1.2	1.7	3.7

be used for predicting large-scale rock processing from the basis of laboratory tests (Ref. 4). It is often used as a comparative measure of the efficiency of rock processing methods-- with lower values of specific energy indicating greater efficiency; but because equipment costs, labor costs, "energy" unit costs, etc., vary for the different methods it can be misleading. For instance, in tunneling, the cost of explosives is a minor cost whereas the costs of drilling holes and "mucking" the rubble are major costs. As another example, flame jet-piercing is economical in many applications in spite of high specific energy values because it utilizes low-cost fuels and has high production rates. Thus, specific energy values, while useful for extrapolating from small-scale to large-scale operations, may be misleading, when used alone, for comparing different methods.

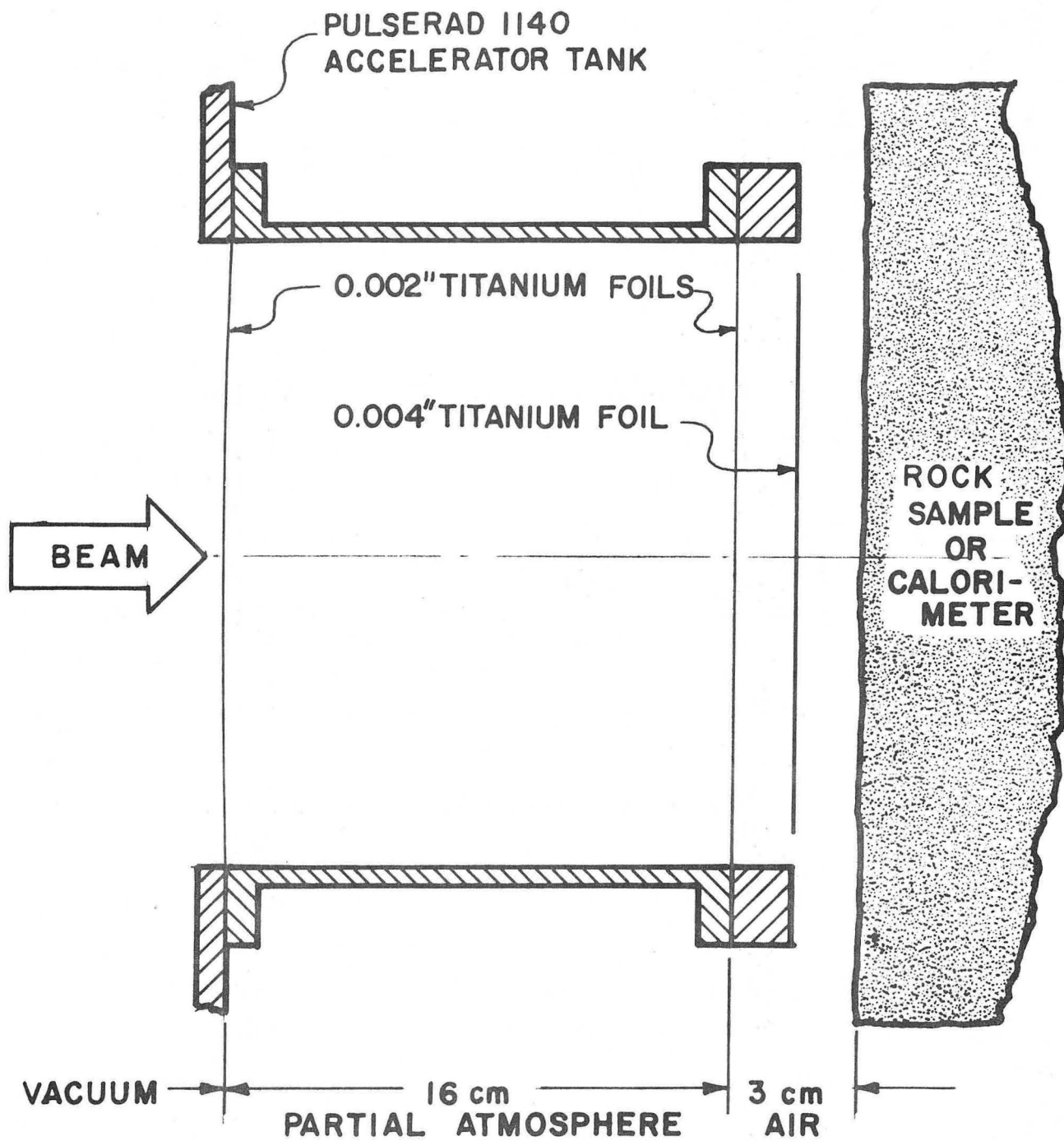
Inspection of Figures 8a and 9a shows that the energy contained in the electrons is not being used with full effectiveness. The energy fluence at the spall radius presumably is the minimum that will produce spalling and can be considered a threshold value. At a small radius the rock received more than the threshold energy deposition while at radii greater than the spall radius some energy has been deposited without producing any spalling. A flatter, sharp-edged electron current distribution should produce substantially more efficient spalling.

3.2.4 Tests Using Pulserad 1140 Accelerator

In November 1973, tests at higher accelerating voltage were conducted using the Pulserad 1140 accelerator located at the San Leandro, California plant of Physics

International Company. The output parameters of this accelerator also are included in Table III. Consultation with the accelerator staff led to the bombardment arrangement shown in Figure 21. The "focusing" or concentration of the electron beam could be adjusted for this accelerator by changing the absolute pressure in the partial atmosphere tank. After some trial, the best operating condition produced energy fluence versus radius as plotted in Figure 22. Compared to the Pulserad 422 accelerator, the beam of the Pulserad 1140 accelerator is considerably more penetrating but has a smaller effective diameter.

A limited number of rocks, mostly wet, were tested. A block of wet basalt bombarded with a single shot produced the results shown in Figure 23. A block of wet granite was similarly bombarded by Shot #18095 followed some minutes later by an adjacent Shot #18096. The resulting spalls and debris are shown in Figure 24. Shot #18096 produced ~ 50% more spall volume than Shot #18095, primarily due to easy removal of the partially fractured material located between the two spalls. The large flakes in the rock debris of these shots comes from the periphery, not the central core, of the spall. The spalls produced by the Pulserad 1140 accelerator appear significantly different than those produced by the lower voltage Pulserad 422 accelerator. This is attributed to the relatively greater penetration depth relative to beam diameter which causes the primary ejected spall to peel off flakes of adjacent material by shear action.



XBL 745-797

Fig. 21. Experimental arrangement at Pulserad 1140 electron accelerator.

SHOT 18099

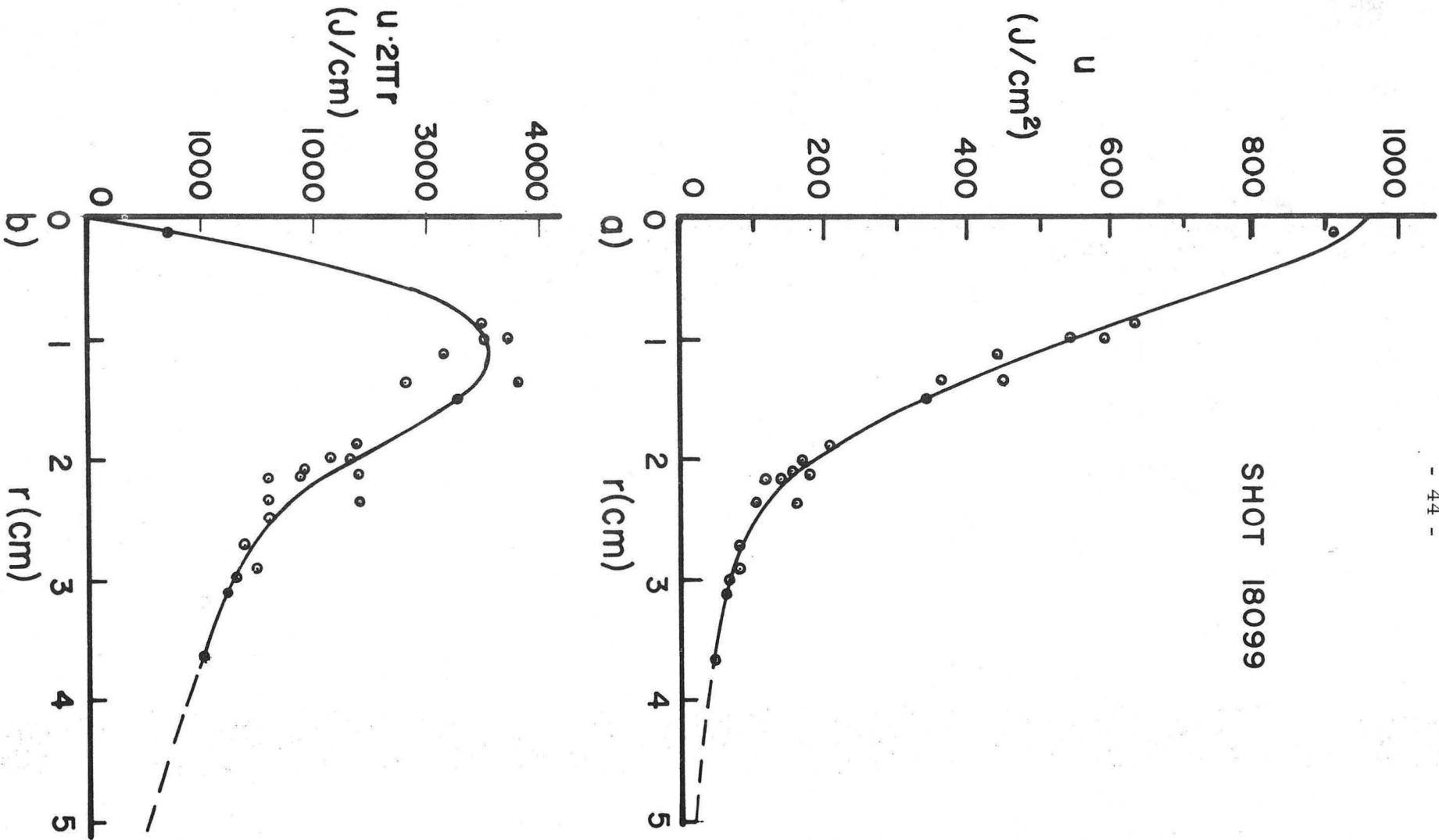


Fig. 22. Typical energy fluence at calorimeter located 3 cm from partial atmosphere chamber of Pulserad 1140 electron accelerator expressed a) in joules per square centimeter of surface and b) in joules per centimeter of radius.



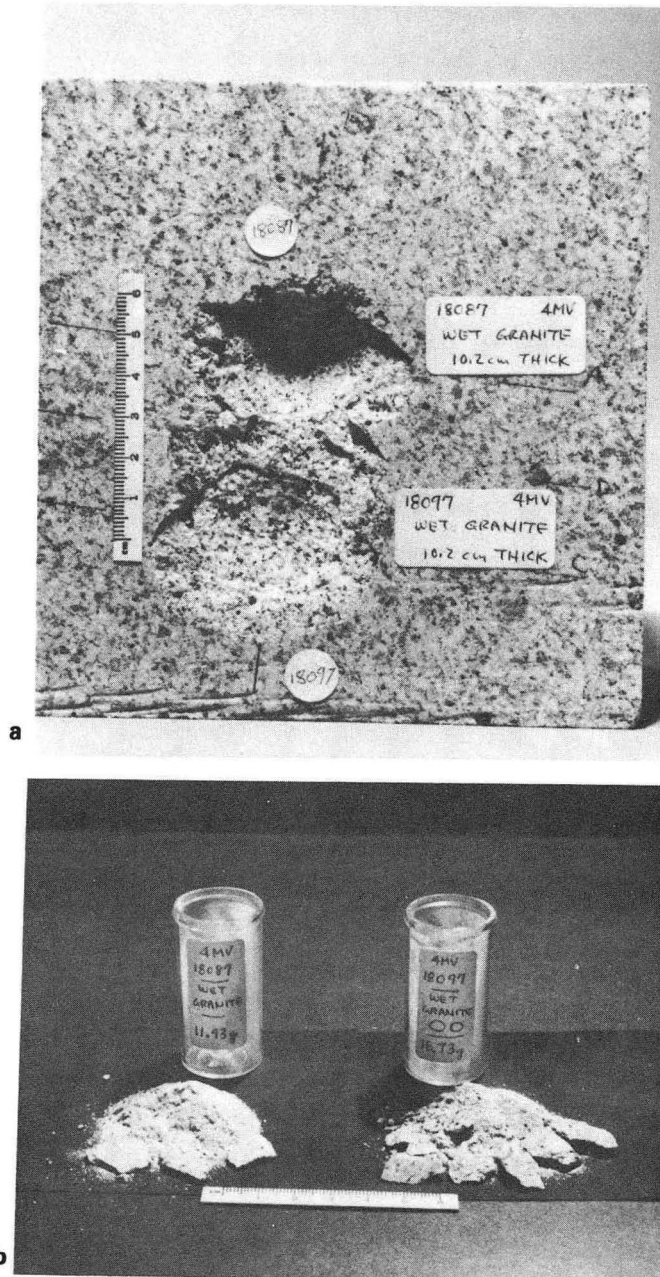
a



b

XBB 744-2851

Fig. 23. a) Wet Napa basalt block 7 cm thick bombarded in air with one shot (5.0 MV, 9.5 kJ, 100 ns) from Pulserad 1140 electron accelerator. b) The spall debris therefrom.



XBB 744-2855

Fig. 24. a) Wet Sierra granite block 10 cm thick bombarded in air with two separate shots (5.0 MV, 9.5 kJ, 100 ns) from Pulserad 1140 electron accelerator. b) The spall debris therefrom.

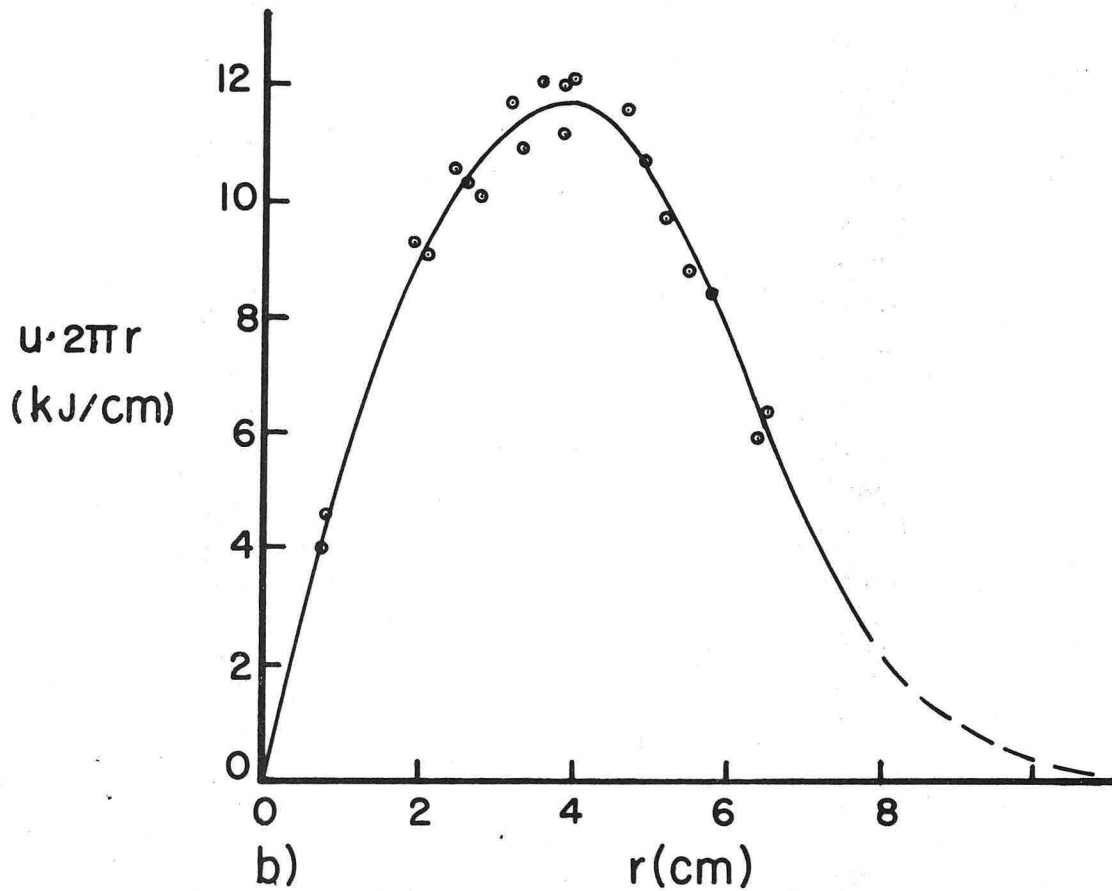
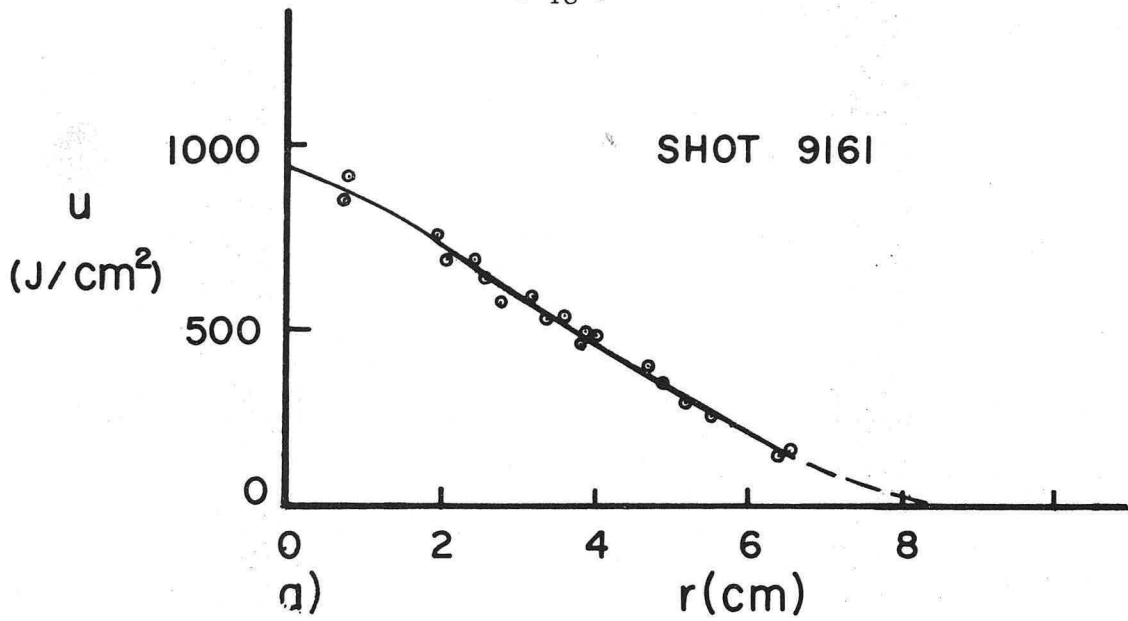
The total volume removed was greater than for the Pulserad 422 accelerator but this is not surprising in view of the greater energy deposition. However, the values of specific energy for these tests were slightly greater than for the Pulserad 422 accelerator. This may be due to beam dispersion while traversing the partial atmosphere tank.

3.2.5 Tests Using Hermes II Accelerator

In January 1974, tests at even higher voltage were conducted using the Hermes II electron accelerator located at Sandia Corporation's Albuquerque, New Mexico facilities. Its output parameters are also listed in Table III. The experimental arrangement was similar to that used at the Pulserad 422 accelerator (shown in Figure 10) except the higher voltage permitted increasing the standoff distance to 18 cm. The energy fluence at this location is shown in Figure 25.

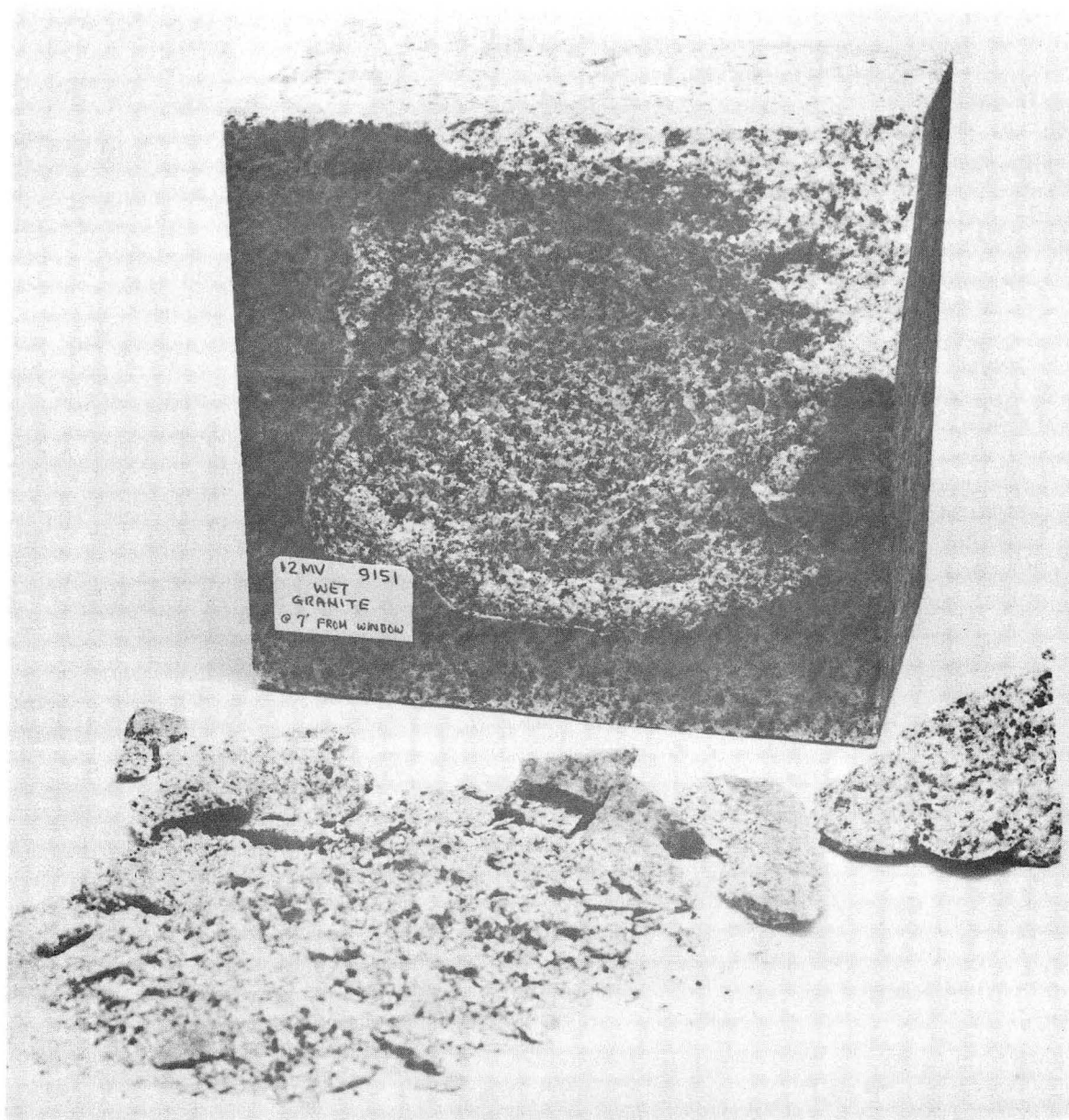
Several rocks were each subjected to a single pulse from the Hermes II accelerator. The results of these bombardments are shown in Figures 26 through 38. Oblique photos showing extensive subsurface cracking adjacent to the spalled zone for Shots 9153, 9154 and 9166 are shown in Figures 28, 31 and 38.

This series of tests demonstrate that a substantial amount of rock can be removed by shock spalling in a single shot. After the test series was underway it became evident that larger-sized rock samples would have been desirable. The removal of the uppermost corners of the rock sample in Shots 9151, 9152 and 9155 probably would not have occurred in a



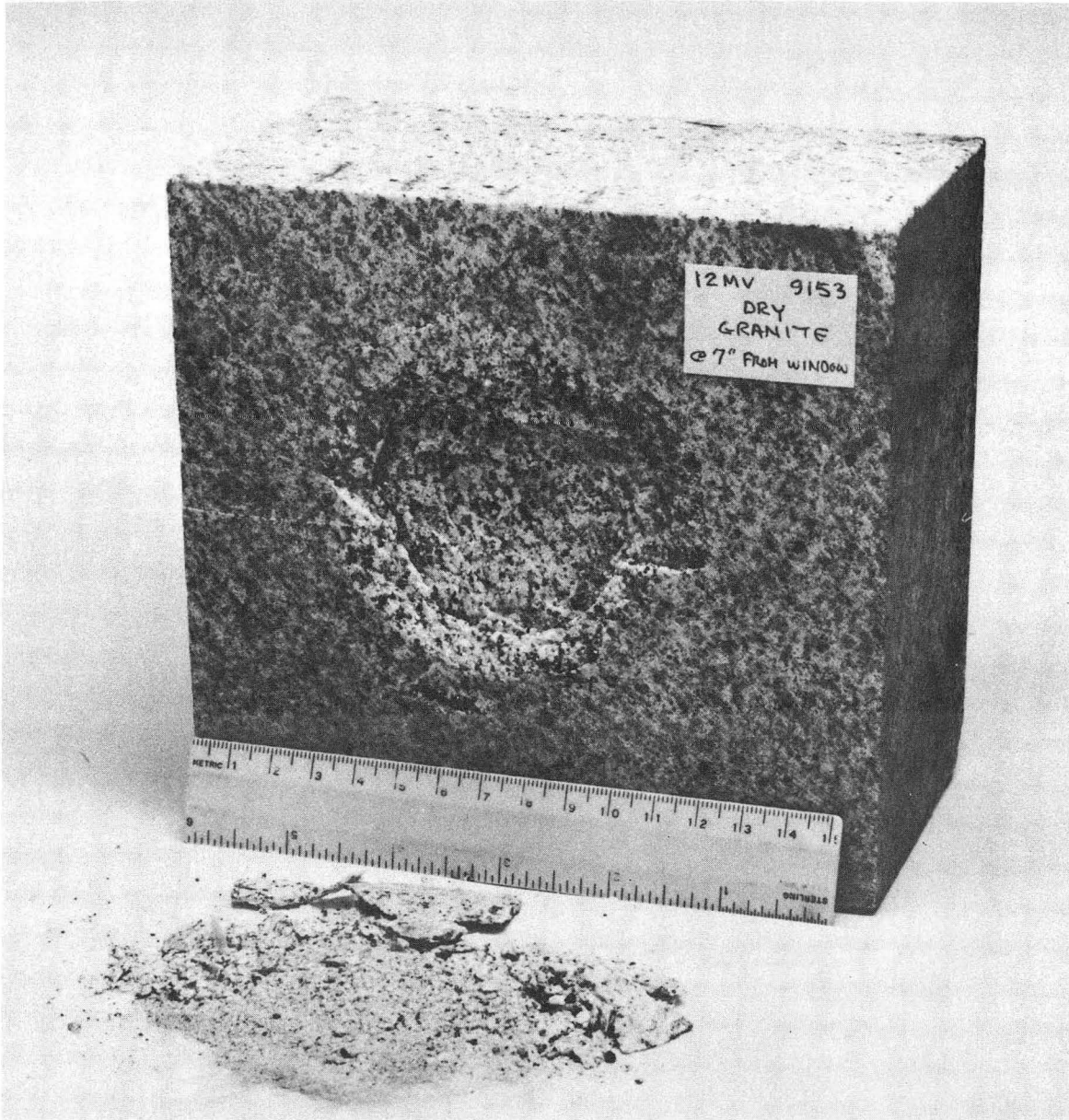
XBL 745-790

Fig. 25. Typical energy fluence at 18 cm from output window of Hermes II electron accelerator expressed a) in joules per square centimeter of surface and b) in kilojoules per centimeter of radius.



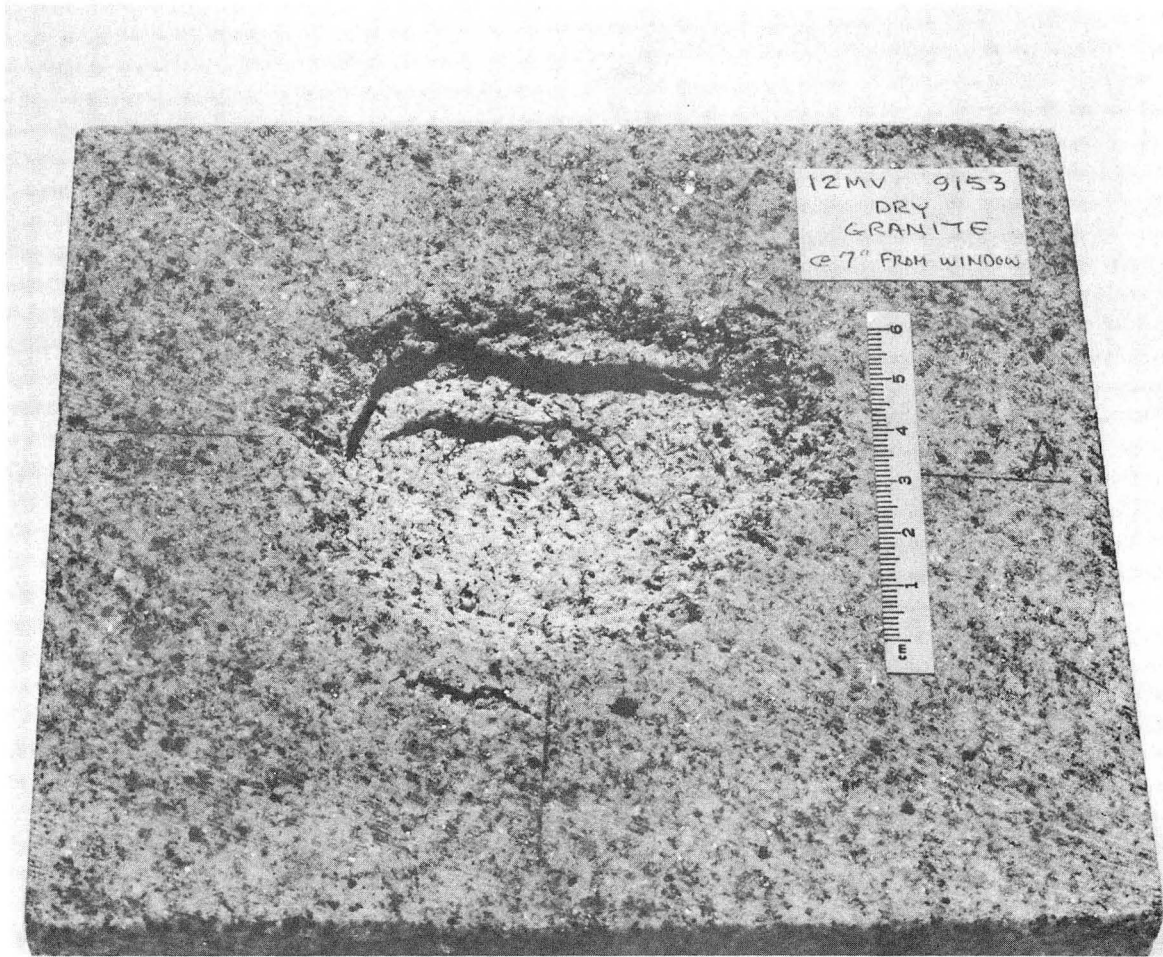
XBL 741-335

Fig. 26. Wet Sierra granite block 10 cm thick bombarded in air with single shot (12.5 MV, 64 kJ, 160 ns) from Hermes II electron accelerator including spall debris therefrom. Larger pieces of debris are from upper edge of block and might not have been removed if the block had been larger.



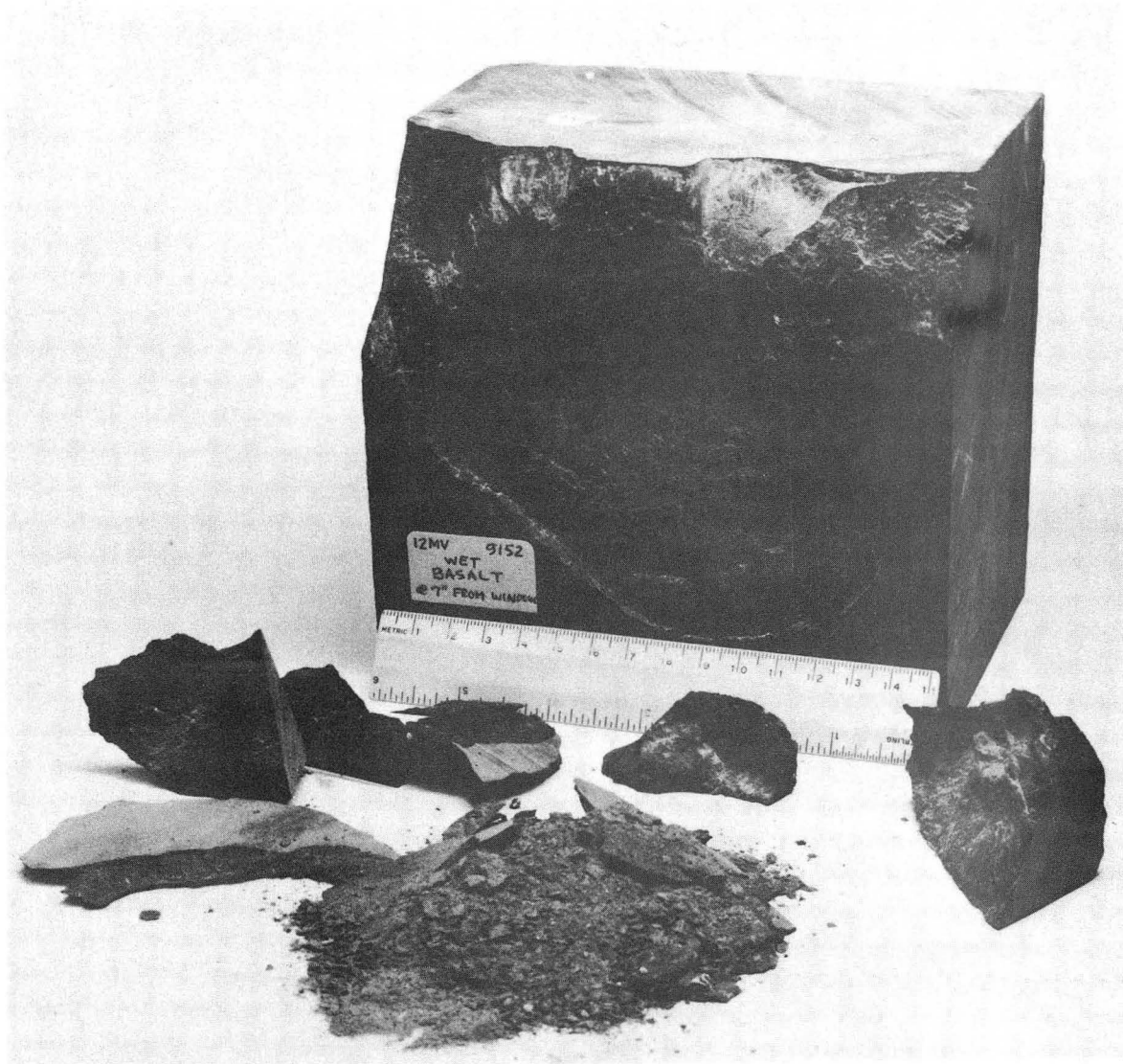
XBB 741-336

Fig. 27. Dry Sierra granite block 9 cm thick bombarded in air with single shot (12.5 MV, 64 kJ, 160 ns) from Hermes II electron accelerator, including spall debris therefrom. Significant subsurface cracks are shown in the next figure.



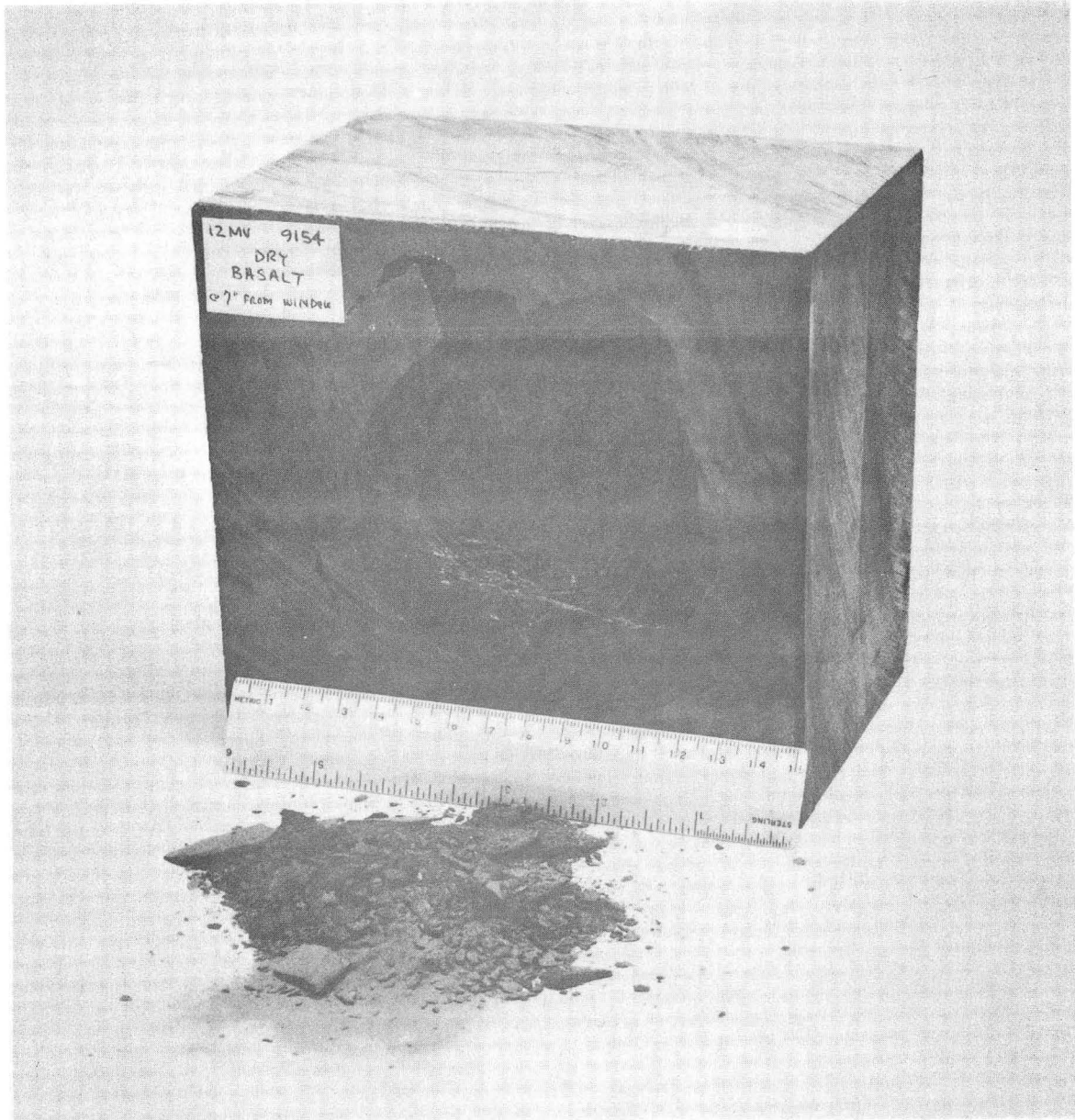
XBB 744-2212

Fig. 28. Oblique view of Shot 9153 onto dry granite showing subsurface cracking.



XBB 741-337

Fig. 29. Wet Napa basalt block 11 cm thick bombarded in air with single shot (12.5 MV, 64 kJ, 160 ns) from Hermes II electron accelerator, including spall debris therefrom. Larger pieces of debris are from upper edge of block and might not have been removed if the block had been larger.



XBB 741-345

Fig. 30. Dry Napa basalt block 11 cm thick bombarded in air with single shot (12.5 MV, 64 kJ, 160 ns) from Hermes II electron accelerator, including spall debris therefrom. Significant subsurface cracks are shown in the next figure.

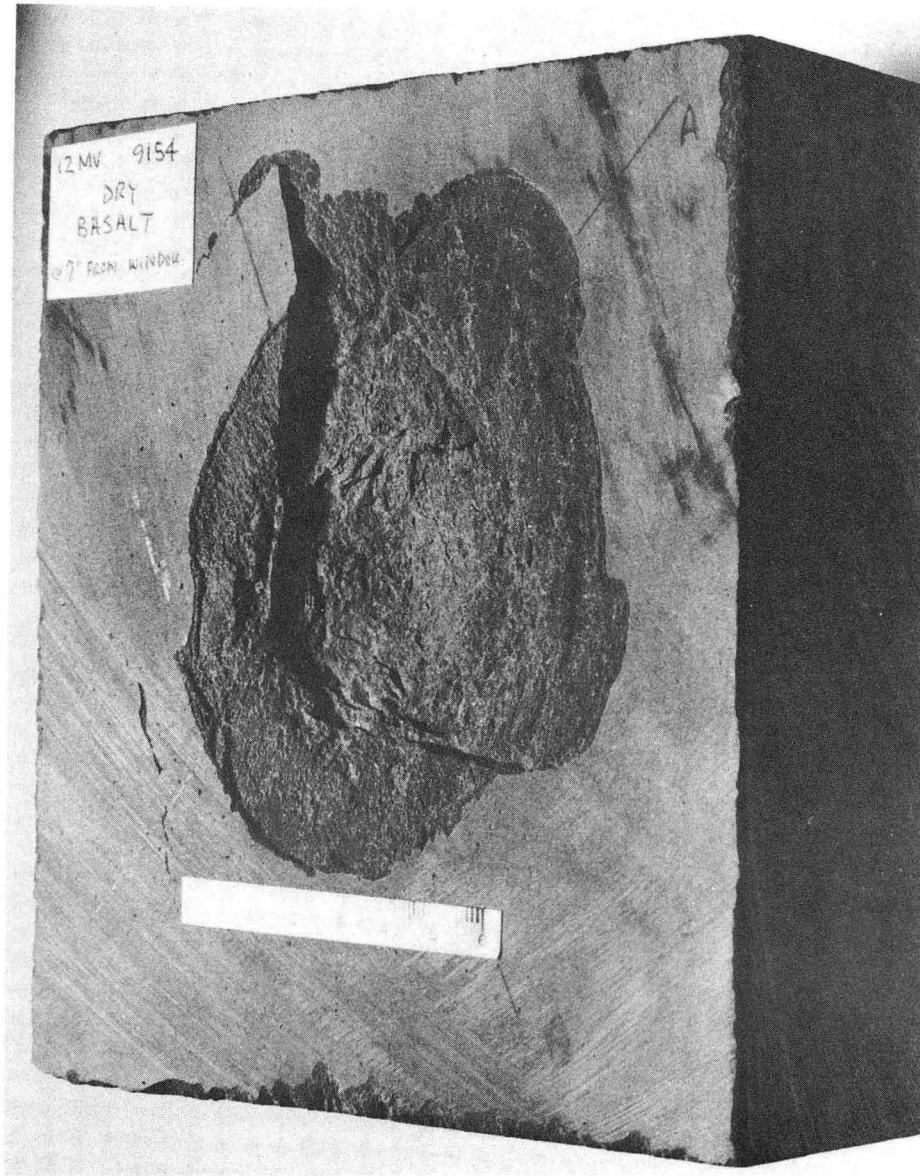


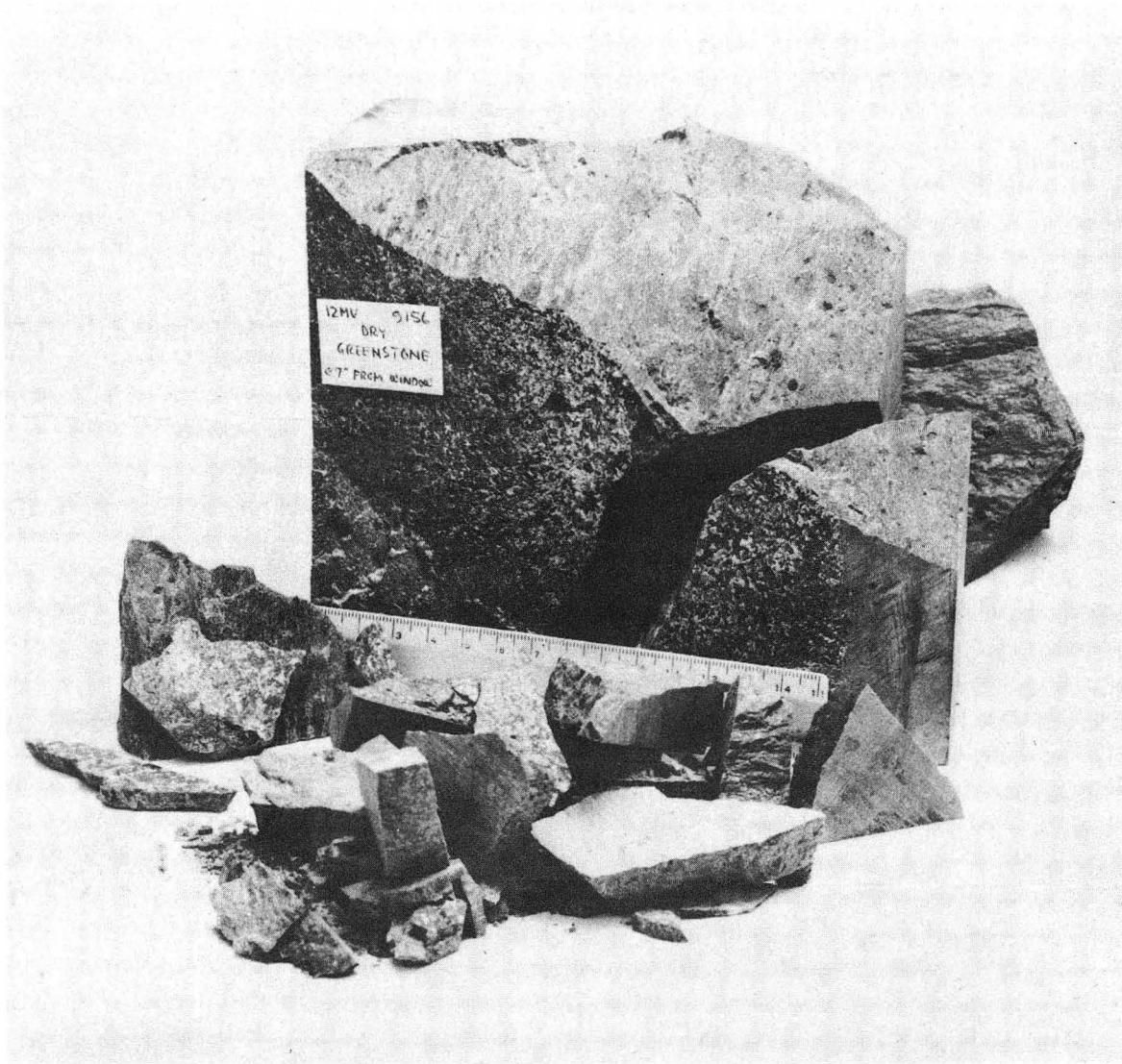
Fig. 31. Oblique view of Shot 9154 onto dry basalt showing subsurface cracking.

XBB 744-2215



XBB 741-344

Fig. 32. Wet greenstone block 11 cm thick bombarded in air with single shot (12.5 MV, 64 kJ, 160 ns) from Hermes II electron accelerator, including spall debris therefrom. Note cracks going through to rear of rock.



XBB 741-344

Fig. 33. Dry greenstone block 10 cm thick bombarded in air with single shot (12.5 MV, 64 kJ, 160 ns) from Hermes II electron accelerator, including spall debris therefrom. Note the extensive fracturing of this block. Earlier tests had shown this rock type to be difficult to spall.



XBB 741-342

Fig. 34. Wet Lyons sandstone block 14 cm thick bombarded in air with single shot (12.5 MV, 64 kJ, 160 ns) from Hermes II electron accelerator, including spall debris therefrom.



XBB 741-341

Fig. 35. Dry Lyons sandstone block 8 cm thick bombarded in air with single shot (12.5 MV, 64 kJ, 160 ns) from Hermes II electron accelerator, including spall debris therefrom. Note horizontal crack at mid-height of block.



XBB 741-340

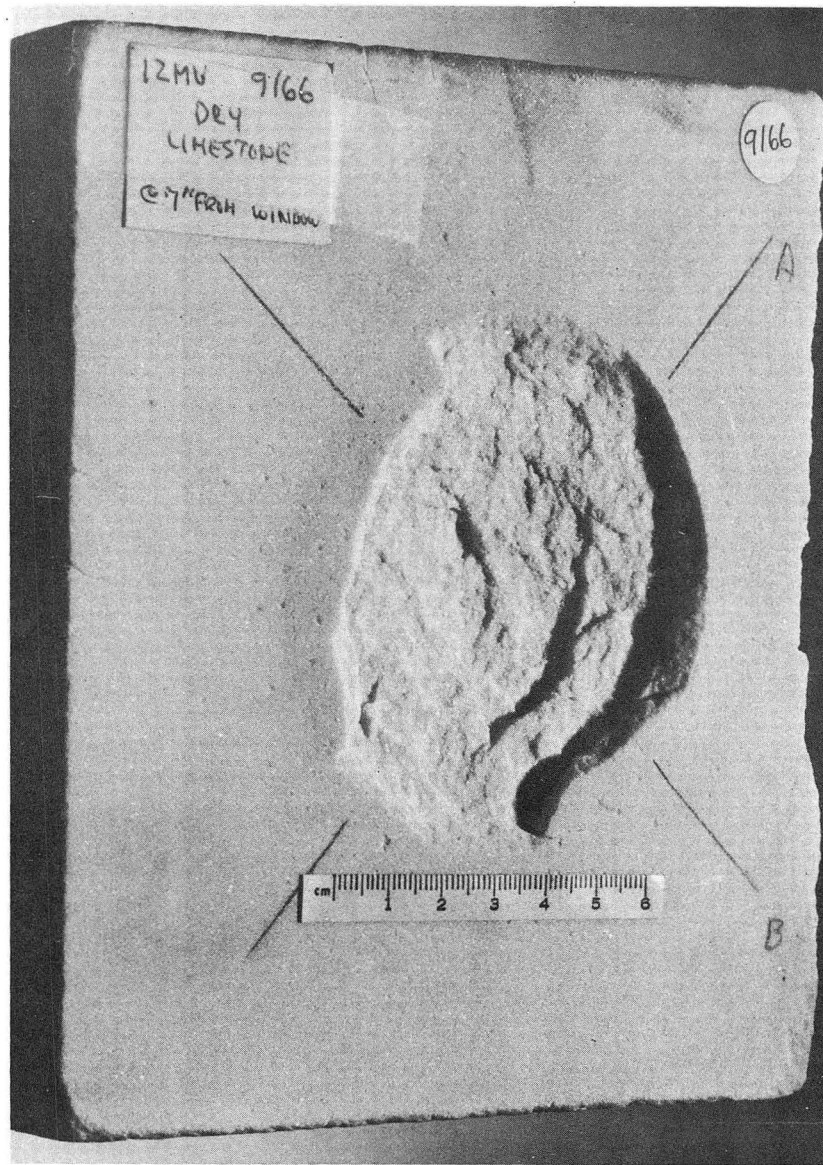
Fig. 36. Wet limestone block 11 cm thick bombarded in air with single shot (12.5 MV, 64 kJ, 160 ns) from Hermes II electron accelerator, including spall debris therefrom.



XBB 741-339

Fig. 37. Dry limestone block 10 cm thick bombarded in air with single shot (12.5 MV, 64 kJ, 160 ns) from Hermes II electron accelerator, including spall debris therefrom. Significant subsurface cracks are shown in the next figure.

Fig. 38. Oblique view of Shot 9166 onto dry white limestone showing subsurface cracking.



XBB 744-2214

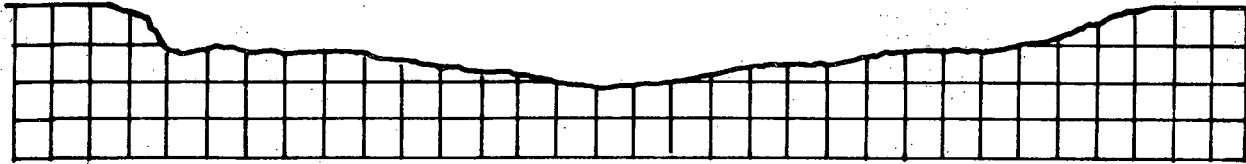
substantially-larger sample. The tests on wet greenstone (Shot 9155) and dry greenstone (Shot 9156) are of particular interest because not only was there a front-surface spall but, in addition, substantial cracking of the remainder of the rock block was produced, particularly in Shot 9156. The greenstone rock was not isotropic and contained partially-healed seams, which probably contributed to the extensive cracking. However, many rocks encountered in tunneling may be similarly anisotropic and may exhibit similarly extensive cracking.

The results of these tests are tabulated in Table VI. For these shots, the average spall diameter was measured directly avoiding regions where corners may have been removed. Spall areas were calculated for circles of the measured diameters. The diametral profiles of the spalls were measured and typical ones are shown in Figure 39. Spall volumes were determined by taking the spall profiles on at least two diameters and then calculating the corresponding volumes of revolution. It is believed that this properly disallows the corner fracturing that occurred on Shots 9151, 9152 and 9155. The internal fracturing on Shot 9155 was not considered in computing the tabulated value of specific energy, however, it is believed that such internal fracturing will lead to substantially greater volume of material removed on subsequent shots in this region. For the greatly shattered greenstone sample in Shot 9156, it is believed unreasonably optimistic to take the total volume of the original rock sample and calculate a corresponding specific energy of only 28 joules/cm^3 . However, no good basis is seen

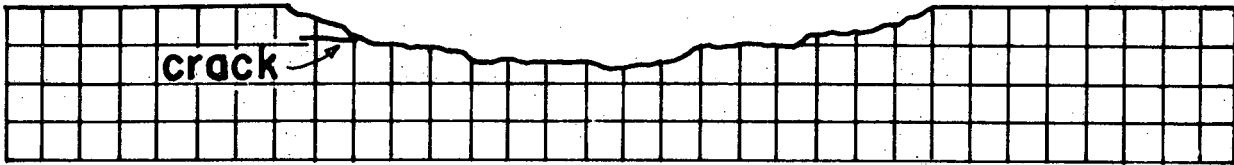
TABLE VI

Single-shot spall data for several tests using Hermes II Accelerator, January 1974.

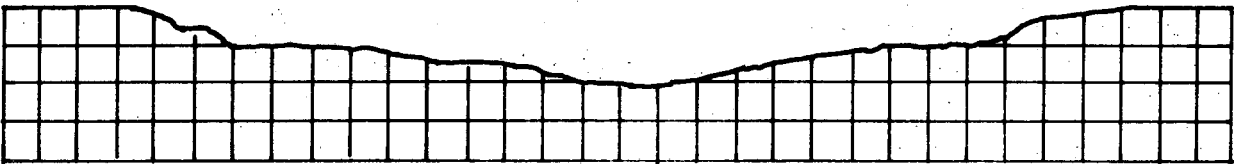
		Colorado Red Sandstone	White Limestone (Marble)	Sierra Granite	Napa Basalt	Greenstone
Compressive strength	MN/m ²	43	58	180	320	270
	10 ³ psi	6	8	26	46	40
Young's modulus of elasticity	GN/m ²	13	41	54	72	99
	10 ⁶ psi	1.9	6	8	10	14
Shot identification number		9163	9165	9151	9152	9155
Mean accelerating voltage	MV	9	9	9	9	9
Standoff distance	cm	18	18	18	18	18
Total energy deposited	kJ	64	64	64	64	64
Spall diameter	cm	12	12	13	13	12
Spall area	cm ²	~ 110	~ 110	~ 130	~ 130	~ 110
Spall depth, max.	cm	1.5	1.1	1.1	1.0	0.7
Volume removed	cm ³	82	57	75	53	51
Specific energy (Energy deposited/volume removed)	kJ/cm ³	0.78	1.11	0.85	1.21	1.25



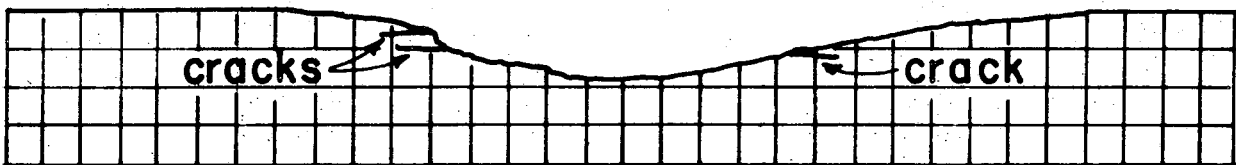
a) Shot 9151 - Wet Sierra granite.



b) Shot 9153 - Dry Sierra granite.



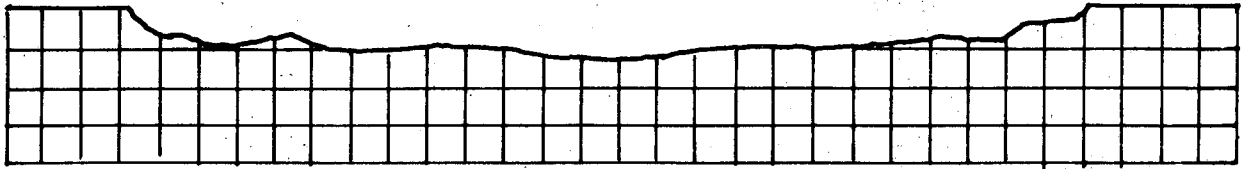
c) Shot 9152 - Wet Napa basalt.



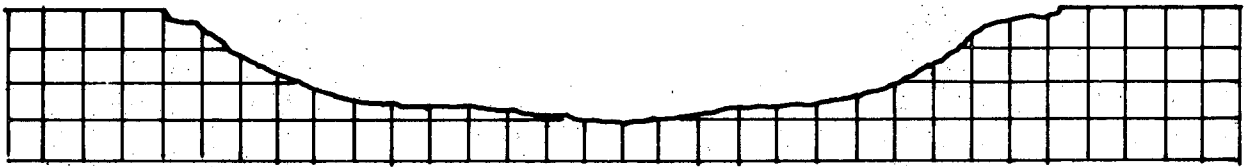
d) Shot 9154 - Dry Napa basalt.

XBL 745-789

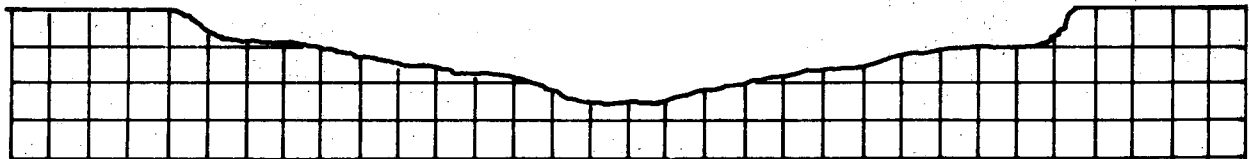
Fig. 39. Profiles through spalls produced by single-shot bombardment of several rocks by Hermes II electron accelerator.



e) Shot 9155 - Wet greenstone. Note relatively uniform depth which suggests that stresswave fracturing mechanism was predominant.



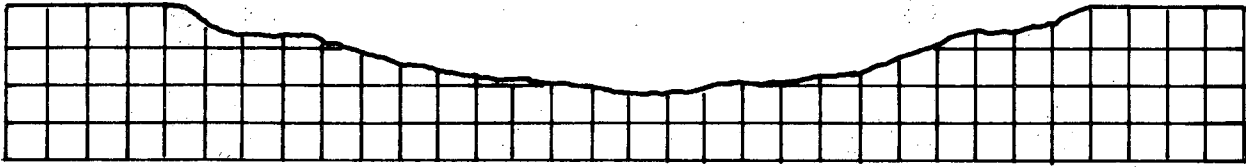
f) Shot 9163 - Wet Lyons sandstone. Note lenticular shape which suggests that thermo-hydraulic fracturing mechanism was predominant.



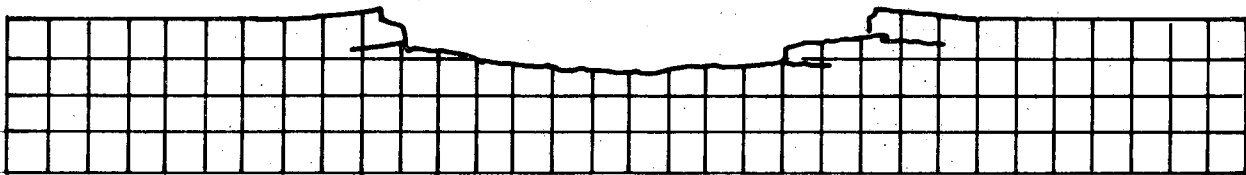
g) Shot 9164 - Dry Lyons sandstone.

XBL 745-788

Fig. 39 (continued)



h) Shot 9165 - Wet white limestone.



i) Shot 9166 - Dry white limestone. Note subsurface cracks and heaving of surface above the cracks.

XBL 745-787

Fig. 39 (continued)

for deciding what fraction of the shattered debris should be considered, so no specific energy value is presented for Shot 9156.

3.2.6 Summary of Experimental Observations

Based on the more than one hundred test shots conducted, the following characteristics of the shock spalling mechanism have been demonstrated:

- 1) It produces spalls on all rock types tested and on clay.
- 2) There is a threshold energy input below which spalling does not occur. The threshold value is primarily a function of rock type and moisture content.
- 3) Generally, the results are reproducible, as shown by repeatable front and rear spalls on identical tests.
- 4) Stronger and tougher rocks generally show less spalling for the same energy input.
- 5) Wet rocks generally show more spalling than dry rocks for the same energy input.
- 6) Wet granite at 0°C, 50°C, and 75°C spalls similarly to wet granite at room temperature.
- 7) Oven-dry granite spalls the same as room-dry granite.
- 8) Rocks bombarded in vacuum also spall.
- 9) The spall size and depth at the front surface are independent of the thickness of the rock sample bombarded (tested only at thicknesses ≥ 2.5 electron penetration depths).
- 10) If the energy fluence of a beam pulse is substantially above threshold for front surface spalling and the

rock sample is thin, spalling can also occur at a rear free surface.

11) Successive nearby pulses (but separated in time by many minutes) generally enhance the spalling process.

12) Greater accelerating voltage produces deeper spalls and generally shows more favorable specific energy.

13) Spall debris is small flakes, sand and dust which should facilitate debris removal by hydraulic slurry or pneumatic means.

14) In several cases, substantial cracking occurred in the rock body outside of the spall zone.

3.3 Analysis and Discussion of the Shock Spalling Technique

The predominant fracturing process is believed to be impulsive thermo-mechanical stressing of the surface layer as described in the immediately following paragraphs. The greater volume and more-finely-divided nature of wet-rock spalls are believed due to an additional thermo-hydraulic fracturing process which is described towards the end of this section.

The main features of the impulsive thermo-mechanical fracturing process can be elucidated by the following somewhat-simplified analysis. Consider a rock face struck by an intense burst of energetic electrons of 50 ns duration with pulse current density of 14 MA/m^2 , mean voltage of 1.0 MV and peak voltage of 1.25 MV. The electrons deposit energy in the rock with a depth dependence approximately as shown in the initial waveform

of Figure 40. The energy is assumed to be deposited uniformly and instantaneously within the volume defined by the beam diameter $2a$ and the density-normalized electron range R (kg/m^2).

The average temperature rise is

$$T_o = \frac{U}{\pi a^2 R c_v} \quad (2)$$

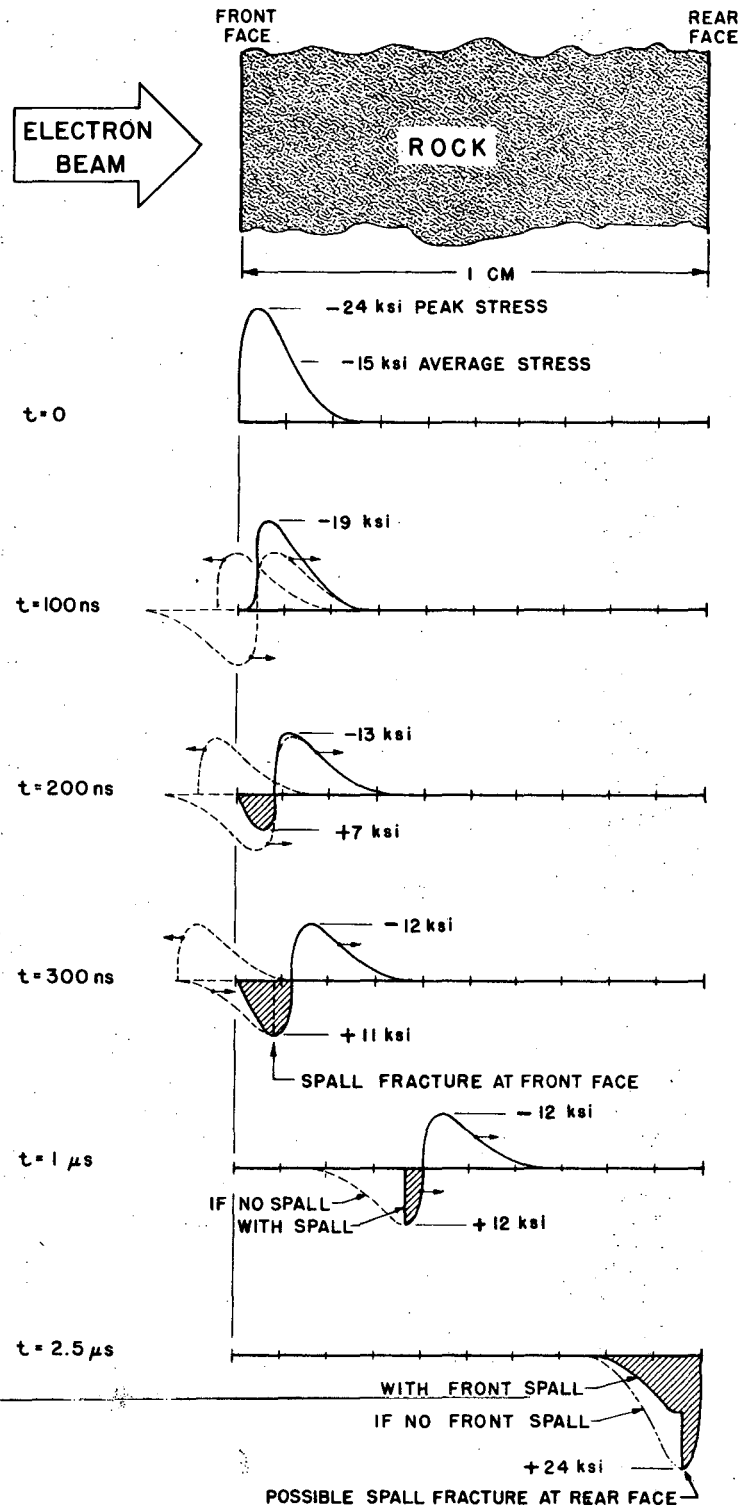
where U is the total energy absorbed in joules per pulse and c_v is the specific heat at constant volume. This temperature rise produces an initial triaxial compressive stress of

$$\sigma_o = \frac{\alpha T_o E}{1 - 2\nu} = \frac{\alpha E U}{(1 - 2\nu) \pi a^2 R c_v} = \Gamma \frac{U \rho}{\pi a^2 R} \quad (3)$$

where α is the thermal coefficient of expansion, E is Young's modulus of elasticity, ν is Poisson's ratio and Γ is the Gruneisen parameter.

For a granite with mechanical properties as given in Table VII, an average temperature rise of 155°C and a corresponding average initial compressive stress of $100 \text{ MN}/\text{m}^2$ ($\sim 15 \text{ ksi}$) are produced in the bombarded zone. The energy deposition is not uniform with depth, as mentioned earlier, so the values will vary from the average values accordingly and the peak temperature rise is $\sim 250^\circ\text{C}$ and the peak compressive stress is $\sim 160 \text{ MN}/\text{m}^2$ (24 ksi).

Following creation of the impulsively stressed volume, elastic stresswaves propagate from the compressed zone. If the electron beam diameter is large compared with the electron



XBL 732-214

Fig. 40. Idealized stresswave propagation within a 1-cm thick rock with wave velocity = 4 km/s. Stress is compressive above baseline and tensile (cross-hatched) below baseline. Wave at $t = 0$ represents initial energy deposition. Dashed lines represent traveling stresswaves whose algebraic sum is the actual stress shown by solid curve. Note the possibility for both a rear spall and a front spall resulting from a single burst of electrons.

TABLE VII

Properties of a competent granite.

Density, ρ	2.7 kg/liter
Thermal coefficient of expansion, α	$7 \times 10^{-6}/^{\circ}\text{C}$
Specific heat, c_v	840 J/kg \cdot $^{\circ}\text{C}$ (0.2 BTU/lb- $^{\circ}\text{F}$)
Modulus of elasticity, E	55 GN/m ² (8×10^6 psi)
Poisson's ratio, ν	0.2
Sonic velocity, $c = \sqrt{E/\rho}$	4 km/s
Compressive strength, σ_c	207 MN/m ² (30,000 psi)
Tensile strength, σ_t	6.2 MN/m ² (900 psi)

penetration depth (R/ρ) the stresswave can be treated as planar and it will propagate in the depth direction as shown in the lower waveforms of Figure 40 (neglecting attenuation and dispersion). The initially-stressed region can be thought to create two oppositely-traveling waves, each of half-magnitude as shown by the dashed curves. The front-going compressive wave is reflected at the free rock face into a rear-going tensile wave. As the waves propagate, a region of the rock at a depth of ~ 1 mm is subjected to a tensile stress of $\sim 80 \text{ MN/m}^2$ (12 ksi) peak magnitude for a fraction of a microsecond. This stress level greatly exceeds the static tensile strength and may result in spalling of the surface layer. If there should happen to be another free surface at moderate depth into the rock face, additional spalling may occur as indicated in the bottom waveform of Figure 40.

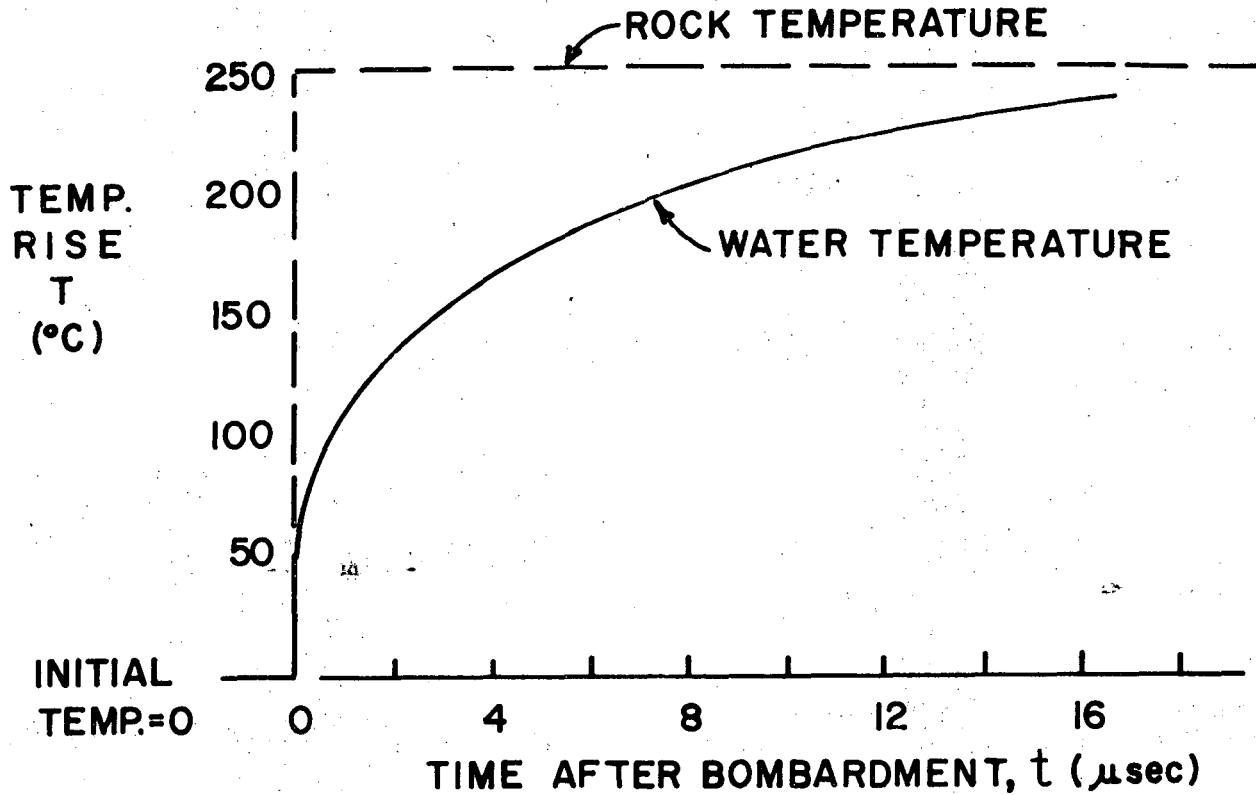
For comparison, when a rock or other brittle material is subjected to static tension, failure typically is characterized by growth of a single crack from a pre-existing major flaw, followed by propagation of the crack over the cross section. The rate of crack propagation approaches a terminal velocity somewhat less than half of the longitudinal sonic wave velocity in the material. In a sense, the weakest point within the rock determines the static tensile strength of the rock.

The shock spalling fracture process is significantly different. As indicated in Figure 40, the traveling stresswaves produce tension at a given location within the rock for only a few tenths of a microsecond. Even if a crack were to start at the

onset of the tensile stresswave and travel at terminal velocity, it could propagate only ~ 1 mm before the wave has passed. This suggests that each small area on the spall surface is fractured substantially independently. A multitude of pre-existing flaws must propagate essentially simultaneously to free the spall from the rock face. The data in Figure 40 and in Table VII indicate that the peak value of the tensile stresswave is approximately an order of magnitude greater than the static tensile strength. In other words, the dynamic tensile strength of rock subjected to submicrosecond tensile pulses appears to be an order of magnitude greater than the static tensile strength. This and the physical appearance of the spalled surface are qualitatively consistent with achieving simultaneous fracture at a multitude of nucleation centers across the spall face.

The following thermo-hydraulic fracturing process is believed to contribute to the spalling of wet rocks. As noted earlier, wet rocks generally show more spalling and also a more finely-divided debris than dry rocks. The somewhat-limited data indicate virtually no difference for greenstone (0.22% porosity), but a marked difference for granite (0.88% porosity), for limestone (0.85% porosity) and for basalt (0.48% porosity). However, sandstone with a very high porosity of 17.8% exhibited only limited enhancement. Under electron bombardment, the energy deposition per unit weight within a water volume is essentially the same as for rock. However, the specific heats are such that if the rock temperature rises 250°C, the intergranular water rises only ~ 50°C during bombardment.

After bombardment, significant heat can be transferred by thermal diffusion from the rock to the water on a microsecond time scale, particularly if the intergranular water layers are only a few micrometers thick as may be the case for the rocks showing the greatest spall enhancement by water. An example of such water heating is calculated in Appendix A and the resulting temperature rise is plotted versus time in Figure 41. Thus, within a few microseconds, the intergranular water temperature may approach the rock temperature. The thermal expansion coefficient of water is about an order of magnitude greater than that typical for many rocks. Consequently, the intergranular water tries to expand more than the surrounding rock and the hydraulic impedance of the internal water paths may be sufficient on this time scale for such water expansion to account for the greater spalling of certain wet rocks. Vaporization of the heated water may account for the greater spall velocity observed in the fast moving pictures. For sandstone, the high porosity suggests that interstitial cracks are relatively large and consequently the water volume therein may take much longer times than a microsecond to be heated significantly and thus exhibit little enhancement when wetted. The foregoing explanations seem qualitatively to fit the experimental observations. Further study of this thermo-hydraulic fracturing process appears warranted.



XBL 745-798

Fig. 41. A calculated example of heating by electron bombardment of water in an interstitial crack. An electron shot at $t = 0$ is assumed to instantaneously raise the rock temperature to $T = 250^{\circ}\text{C}$ and the water to $T = 50^{\circ}\text{C}$, the difference being due to differing specific heats. Subsequently, heat diffuses from the rock into the water and the curve shows the water temperature rise in a $3 \mu\text{m}$ crack assuming the thermal diffusivity of the rock is much greater than for water. Note the significant heat transfer on a micro-second time scale.

4. PROSPECTS FOR THE FUTURE

Tunneling, mining and other excavation in rock are promising applications for the shock spalling technique although it is clear that additional research and engineering are needed. The national need to reduce the cost and increase the speed of underground excavation and tunneling is well known (Ref. 16). The specific energy levels reported herein may be low enough for economic feasibility, but even lower values appear likely. Beam parameters not yet tested may produce more efficient spalling. Lateral compressive stresses due to residual heat during high-repetition-rate bombardment as well as those generally prevailing in in-situ rock may enhance the shock spalling efficiency. Also, residual damage from earlier pulses should enhance spalling during repetitive bombardment. In addition, a variety of strategies for using shock spalling in combination with other methods can be considered, such as cutting a pattern of grooves by shock spalling followed by removal of intermediate material by mechanical means. These improvement factors lead to the expectation of specific energies in the range of 100 to 1,000 joules/cm³ or perhaps lower.

The prospects appear promising for technical and economic feasibility of a Pulsed Electron Tunnel Excavator capable of tunnel advance rates approaching 75 meters (~ 250 feet) per day through hard rock. This compares to conventional tunneling rates through hard rock of the order of 10 to 15 meters (~ 30 to 50 feet) per 24-hour day under favorable conditions. The following paragraphs set forth initial findings regarding the feasibility

of such an excavator. A more detailed evaluation of such a system is being conducted at this writing.

A simplified conceptual sketch of a Pulsed Electron Tunnel Excavator is shown in Figure 42. The accelerator proper is pictured as housed within a steel tank perhaps 25 meters (82 feet) long. Tentative output performance parameters of the electron accelerator are set forth in Table VIII and appear achievable. The physical size of the equipment may seem large, but so are existing tunneling "moles." It could conveniently fit in a 3.5 meter (11.5 feet) diameter tunnel and perhaps into one of 2.5 meter (8.2 feet) diameter or less. On the front would be mounted a system for a combination of both magnetic and mechanical scanning of the beam across the rock face. Bringing the electrons out from the high vacuum of the accelerator into the tunnel air is a significant problem, but some possible solutions have already been evolved. The beam will travel through air for a distance of perhaps 2 to 20 cm (0.8 to 8 inches) to reach the rock face. As now pictured, the accelerator and beam scanner would be on one vehicle followed immediately by another vehicle containing auxiliary equipment, switchgear and the operators cab. The accelerator and auxiliary vehicle can be ruggedly built to survive in the hostile tunnel environment. Naturally, there would need to be provision for other tunneling functions such as lining, shields, rock bolting, etc. as may be required.

Radiation safety requirements appear easily met. The machine produces radiation only when it is running. The

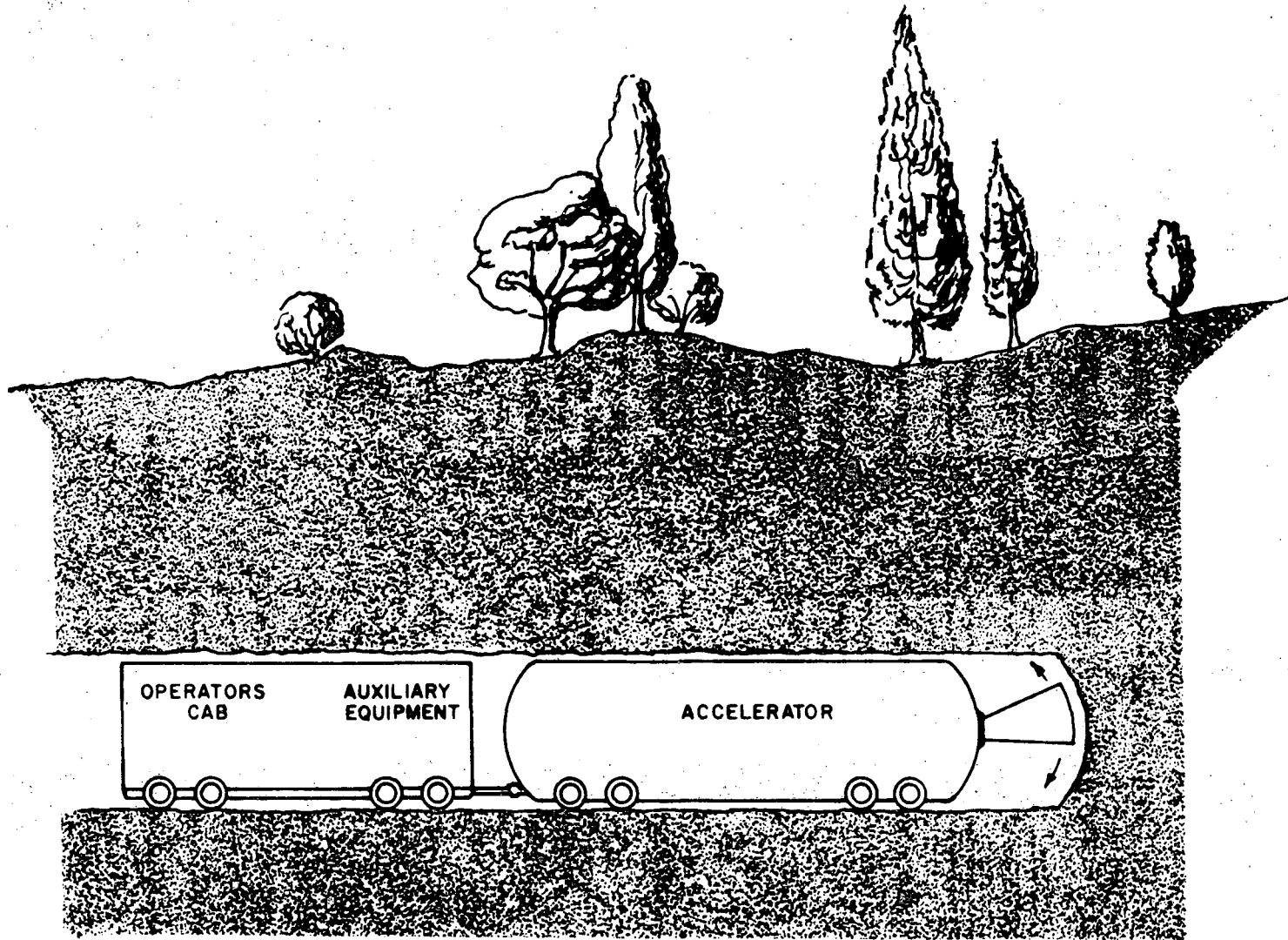


Fig. 42. Simplified conceptual sketch of an accelerator for rock excavation. Shields and tunnel lining are not shown.

XBL 745-802

TABLE VIII

Tentative performance parameters for
Pulsed Electron Tunnel Excavator.

Excavation volume per hour*	104	m ³ /hr
Specific energy (assumed)	500	J/cm ³
Beam power, average	14.4	MW
Beam voltage	5	MV
Rep rate	720	Hz
Energy per pulse	20	kJ
Charge per pulse	4	mC
Pulse duration	1.0	μs
Pulse current	4	kA
Spall depth, average	~ 0.4	cm
Spall diameter	~11	cm
Spall volume per pulse	40	cm ³
Overall electrical efficiency	>50	%

*This corresponds to excavation of a 21-foot (6.4 m) diameter tunnel at the rate of 10.6 feet (3.22 m) per hour.

operating crew can be protected by shielding built into the accelerator vehicle while the general public is protected by the rock over-burden. Induced radioactivity is not a problem if the beam voltage is below five megavolts or so.

The spall debris is sand, small flakes and dust which can be easily removed from the rock face to the rear of the accelerator by a suction pipe. This might be coupled with the tunnel ventilation system. Alternatively, the debris might be removed by hydraulic slurry piping. The water brought in for hydraulic slurry handling can also be used for cooling the equipment and the debris--a significant problem for any rapid-advance technique.

The cost of electricity for this machine is comparatively small at today's tunneling costs (but the same can be said for dynamite). The capital cost of accelerator equipment, as well as personnel and maintenance costs, will likely determine the economic feasibility of this concept, and appear promising at this writing.

On a much smaller scale, shock spalling might be used for "machining" of ceramic turbine blades and other brittle materials. As an immediate application, these very-short duration stress pulses can provide information on the fundamental nature of fracture initiation and crack propagation in brittle materials.

5. CONCLUSIONS

This study of rock shattering using intense bursts of energetic electrons has opened up the possibility of a new type of tunneling technique. It would be premature to draw conclusions about its use in practical operations. The study reported herein has led to the following results:

1. The "thermal crater" fracturing process, which involves taking at least many microseconds to deposit an electron pulse, does not appear attractive. The tests indicate cracking occurs only for certain rocks and then only after much energy has been deposited.

2. The "shock spalling" process, which involves depositing an electron pulse generally in less than a microsecond of time, produces an explosive-like ejection of a significant portion of the bombarded rock volume. The debris is of fine nature which can facilitate its removal. Wet rocks generally show greater and finer spalling than dry rocks. Shock spalling was successfully produced in all of a variety of rock types tested, ranging from very hard to soft, and even clay. The energy deposited in the rock corresponds to a temperature rise of only a small fraction of its melting temperature.

3. The shock spalling process holds considerable promise for practical application in the tunneling industry. Electron accelerators of suitable output can be built for this application, although development work is needed on electron delivery techniques. The accelerator can be housed within a steel enclosure for protection from the hostile tunnel environment. The fine

debris can be handled by hydraulic slurry or pneumatic means. The process can convert hard-rock tunneling into a continuous process rather than the conventional batch technique.

4. Studies of the shock spalling process and application of the process to a practical Pulsed Electron Tunnel Excavator are continuing. There is need for construction of a rapid-fire pulsed electron accelerator to determine the spall enhancement that can be achieved by rapid repetitive electron bombardment and to develop components suitable for delivering the electron pulses to a rock face. Such an accelerator would facilitate proof of the practicality of the shock spalling technique.

ACKNOWLEDGMENTS

Thankful acknowledgment is extended to the National Science Foundation for financial support under NSF Grant AG-393 and to the U. S. Atomic Energy Commission and the Lawrence Berkeley Laboratory for use of facilities and support. The support of these agencies was essential to the progress of the work described herein.

Appreciation is extended to the large number of people at the Lawrence Berkeley Laboratory, the Lawrence Livermore Laboratory, the University of California at Berkeley, Physics International Company, Sandia Corporation, and at other institutions, whose work and cooperation have contributed to this study. Special appreciation is given to Professors Iain Finnie and Tor L. Brekke of the College of Engineering at the University of California and to Dr. Denis Keefe of the Lawrence Berkeley Laboratory for their advice concerning the work described herein. The helpful guidance of Dr. Ralph Long and Dr. W. W. Hakala as Program Managers for NSF has been appreciated. Thanks are due to Mrs. Maggie Petersen for the typing of this dissertation.

REFERENCES

1. R. Avery, et al., "The ERA 4 MeV Injector, "IEEE Trans. Nucl. Sci., NS-18, No. 3 (June 1971).
2. R. T. Avery, "On the Possibility of Rock Fracture by Intense Bursts of Energetic Electrons, " UCID-3522 (1971).
3. The term "shock spalling" was selected to describe rock spalling due to very-short-duration electron beam deposition and to distinguish it from the more conventional static and quasi-static spalling mechanisms. The stresswaves produced are believed to be elastic and not possess the wavefront characteristics of shockwaves, with which they should not be confused.
4. W. C. Maurer, "Novel Drilling Techniques." Pergamon Press, (1968).
5. B. W. Schumacher and C. R. Taylor, "Rock Breakage by Means of Electron Beam Piercing." Record of 10th Symposium on Electron, Ion, and Laser Technology (L. Marton, Ed.); San Francisco Press, Inc., (1969).
6. B. W. Schumacher, "Electron Beam Cutting of Rocks and Concrete." Electron and Ion Beam Science and Technology, Third Intl. Conf., R. A. Bakish, Ed., The Electrochemical Society, New York, (1968).
7. B. W. Schumacher and R. G. Holbrook, "Use of Electron Beam Gun for Hard Rock Excavation." Final Technical Report Bu Mines/ARPA Contract H 0110377 (1972).

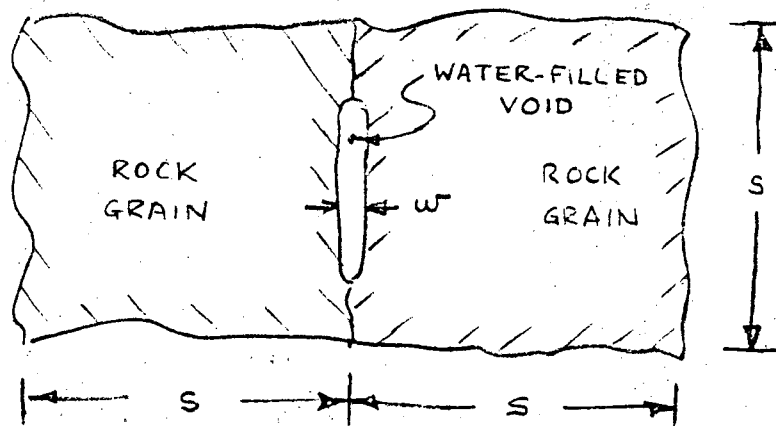
8. J. P. Carstens, et al., "Research Investigation of Laser Rock Kerfing." United Aircraft Research Labs Report L-911329-8. NITS Report FRA-RT-73-12. (1972).
9. R. T. Avery, D. Keefe, T. L. Brekke and I. Finnie, "Shattering Rock with Intense Bursts of Energetic Electrons." IEEE Trans. on Nucl. Sci., Vol. NS-20, No. 3 (June 1973). (Proceedings of 1973 Particle Accelerator Conference, San Francisco, Calif., March 5-7, 1973.) Also published as preprint report LBL-1391 (1973).
10. R. T. Avery, D. Keefe, T. L. Brekke and I. Finnie, "Use of Intense Sub-Microsecond Electron Bursts to Produce Rock Shattering." Accepted for 3rd Int. Congress on Rock Mechanics, Denver, Colorado, Sept. 1-7, 1974. Also published as preprint report LBL-2137 (Jan. 1974).
11. R. T. Avery, et al., "Proposal for Study of Rock Shattering by Intense Bursts of Energetic Electrons." Lawrence Berkeley Laboratory and University of California, unpublished (1971).
12. Computations by O. Vardar using finite-element static stress programs developed by the Structural Engineering Laboratory, University of California, Berkeley (1972).
13. H. S. Carslaw and J. C. Jaeger, "Conduction of Heat in Solids." Section 7.9, Oxford Press, 1959.
14. Gregg E. Korbin and Tor L. Brekke, "Summary of Rock Property Data for the Study of Rock Shattering by Intense Bursts of Energetic Electrons." University of California Berkeley, College of Engineering Internal Report UCX-2437. (1972).

15. J. W. Beal, N. C. Christofilos and R. E. Hester, "The Astron Linear Accelerator." IEEE Trans. Nucl. Sci. NS-16, No. 3, p. 294 (June 1969).
16. R. F. Baker, et al., "The Use of Underground Space to Achieve National Goals." Underground Construction Research Council of ASCE/AIME. New York, N.Y. (1972).

APPENDIX A

Electron Bombardment Heating
of Interstitial Water

When an energetic electron beam passes through matter, the energy deposited in a given small volume is proportional to density, to a good approximation.



Consider an interface between two grains with a water-filled void of thickness w . Upon electron bombardment, the instantaneous temperature of the rock grain is T_{or} and of the water is T_{ow} . Due to the difference in specific heats, $T_{ow} \approx 0.2 T_{or}$.

If $w \ll s$, the heat transfer can be approximated as one-dimensional (perpendicular to interface). This appears valid except near the grain corners.

The thermal diffusivity of rocks typically is large compared to that of water (Ref: Carslaw & Jaeger, Appendix VI). Therefore, to a first approximation, the rock can be considered as a heat source maintained at temperature T_{or} .

Consider thermal diffusion of heat into the water volume from the rock. Convection, boiling or other mass transfer phenomenon are not considered since they appear unlikely to be significant on a microsecond time scale. Thermal conduction is considered as the only heat transfer mechanism through the water.

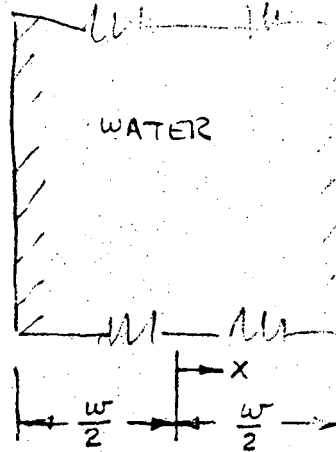
Boundaries: Parallel planes

B.C.:

$$\text{at } x = \pm \frac{w}{2}, T = T_{\text{or}} \\ \text{for } t > 0$$

I.C.:

$$\text{at } t = 0, T = T_{\text{ow}}$$



This case has been considered by Carslaw & Jaeger, "Conduction of Heat in Solids," 2nd Ed., Section 3.4, who give the solution as

$$\frac{V}{V_0} = 1 - \frac{4}{\pi} \sum_{n=0}^{\infty} \frac{(-1)^n}{2n+1} e^{-\frac{(2n+1)^2 \pi^2 \tau}{4}} \cdot \cos \frac{(2n+1)\pi \xi}{2}$$

where

$$V = T - T_{\text{ow}}$$

$$V_0 = T_{\text{or}} - T_{\text{ow}}$$

$$\tau = \frac{t}{l^2}$$

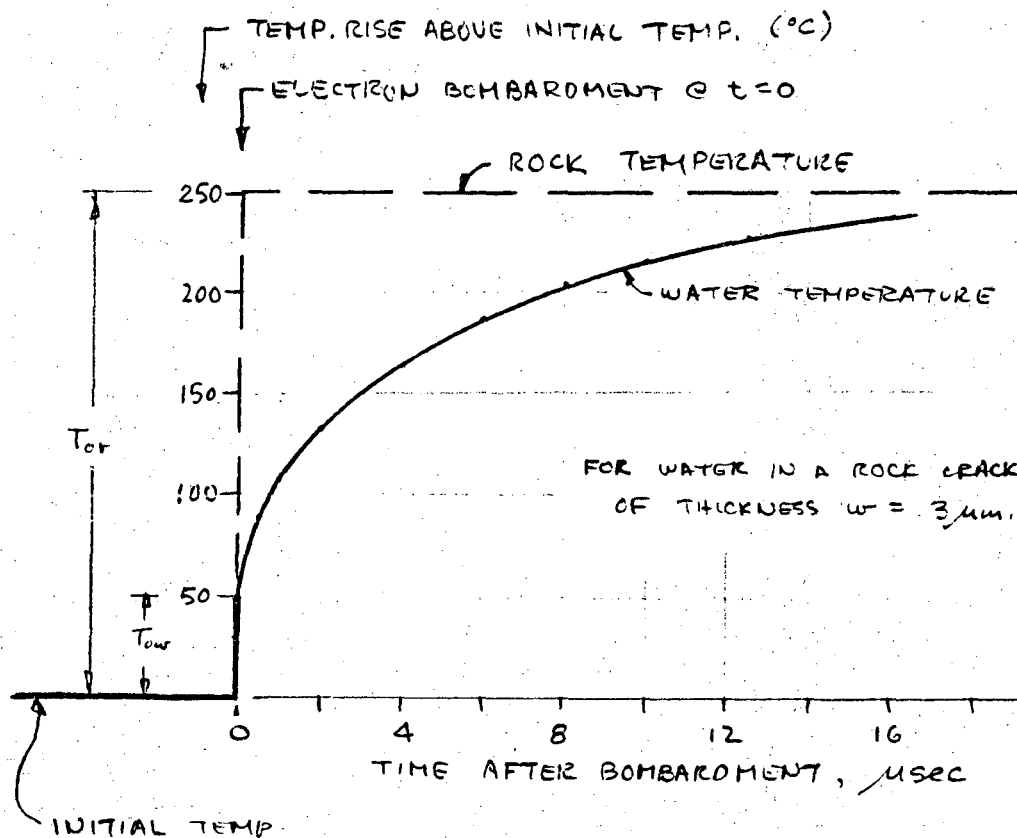
$$\xi = \frac{x}{l}$$

$$l = \frac{w}{2}$$

They also present graphs (Figures 11 and 12) giving numerical values based on the foregoing equation. One graph presents temperature profiles versus depth at successive time increments while the other graph presents both the central temperature (at $x = 0$) and the average temperature (averaged through thickness) as a function of time.

As an illustration, consider a case with an interstitial crack with total thickness $w = 3 \mu\text{m}$ containing water whose thermal diffusivity $\kappa = 1.44 \times 10^{-7} \text{ m}^2/\text{s}$. Due to electron bombardment at $t = 0$, assume the instantaneous temperature of the rock is $T_{or} = 250^\circ\text{C}$ and of the water is $T_{ow} = 50^\circ\text{C}$, both relative to a pre-bombardment temperature of $T_o = 0^\circ\text{C}$.

Using Figure 12 from Carslaw and Jaeger, the mean water temperature versus time is



This indicates that significant amounts of heat can be transferred to the water in times as short as one microsecond for this case. Since the characteristic heat transfer time varies as w^{-2} , water in thinner cracks will heat even more rapidly.

LEGAL NOTICE

This report was prepared as an account of work sponsored by the United States Government. Neither the United States nor the United States Atomic Energy Commission, nor any of their employees, nor any of their contractors, subcontractors, or their employees, makes any warranty, express or implied, or assumes any legal liability or responsibility for the accuracy, completeness or usefulness of any information, apparatus, product or process disclosed, or represents that its use would not infringe privately owned rights.

TECHNICAL INFORMATION DIVISION
LAWRENCE BERKELEY LABORATORY
UNIVERSITY OF CALIFORNIA
BERKELEY, CALIFORNIA 94720